NeuroImage: Clinical 41 (2024) 103577

Contents lists available at ScienceDirect

NeuroImage: Clinical

journal homepage: www.elsevier.com/locate/ynicl

Increased iron in the substantia nigra pars compacta identifies patients with early Parkinson's disease: A 3T and 7T MRI study

Erind Alushaj [a,b], Nicholas Handfield-Jones [a,b], Alan Kuurstra [c,d], Anisa Morava [e], Ravi S. Menon [c,d], Adrian M. Owen [b,f], Manas Sharma [g,h], Ali R. Khan [c,d], Penny A. MacDonald [b,h,*]

[a] Department of Neuroscience, Schulich School of Medicine and Dentistry, Western University, London, Ontario N6A 3K7, Canada
[b] Western Institute for Neuroscience, Western University, London, Ontario N6A 3K7, Canada
[c] Robarts Research Institute, Western University, London, Ontario N6A 3K7, Canada
[d] Department of Medical Biophysics, Western University, London, Ontario N6A 3K7, Canada
[e] School of Kinesiology, Faculty of Health Sciences, Western University, London, Ontario N6A 3K7, Canada
[f] Department of Physiology and Pharmacology, Western University, London, Ontario N6A 3K7, Canada
[g] Department of Radiology, Western University, London, Ontario N6A 3K7, Canada
[h] Department of Clinical Neurological Sciences, Western University, London, Ontario N6A 3K7, Canada

ARTICLE INFO

Keywords:
Parkinson's disease
Neuroimaging
Quantitative susceptibility mapping
Iron
Midbrain

ABSTRACT

Degeneration in the substantia nigra (SN) pars compacta (SNc) underlies motor symptoms in Parkinson's disease (PD). Currently, there are no neuroimaging biomarkers that are sufficiently sensitive, specific, reproducible, and accessible for routine diagnosis or staging of PD. Although iron is essential for cellular processes, it also mediates neurodegeneration. MRI can localize and quantify brain iron using magnetic susceptibility, which could potentially provide biomarkers of PD.

We measured iron in the SNc, SN pars reticulata (SNr), total SN, and ventral tegmental area (VTA), using quantitative susceptibility mapping (QSM) and R2* relaxometry, in PD patients and age-matched healthy controls (HCs). PD patients, diagnosed within five years of participation and HCs were scanned at 3T (22 PD and 23 HCs) and 7T (17 PD and 21 HCs) MRI. Midbrain nuclei were segmented using a probabilistic subcortical atlas. QSM and R2* values were measured in midbrain subregions. For each measure, groups were contrasted, with Age and Sex as covariates, and receiver operating characteristic (ROC) curve analyses were performed with repeated *k*-fold cross-validation to test the potential of our measures to classify PD patients and HCs. Statistical differences of area under the curves (AUCs) were compared using the Hanley-MacNeil method (QSM versus R2*; 3T versus 7T MRI).

PD patients had higher QSM values in the SNc at both 3T ($p_{adj} = 0.001$) and 7T ($p_{adj} = 0.01$), but not in SNr, total SN, or VTA, at either field strength. No significant group differences were revealed using R2* in any midbrain region at 3T, though increased R2* values in SNc at 7T MRI were marginally significant in PDs compared to HCs ($p_{adj} = 0.052$). ROC curve analyses showed that SNc iron measured with QSM, distinguished early PD patients from HCs at the single-subject level with good diagnostic accuracy, using 3T (mean AUC = 0.83, 95 % CI = 0.82–0.84) and 7T (mean AUC = 0.80, 95 % CI = 0.79–0.81) MRI. Mean AUCs reported here are from averages of tests in the hold-out fold of cross-validated samples. The Hanley-MacNeil method demonstrated that QSM outperforms R2* in discriminating PD patients from HCs at 3T, but not 7T. There were no significant differences between 3T and 7T in diagnostic accuracy of QSM values in SNc.

Abbreviations: ANTs, Advanced Normalization Tools; AUC, Area under the curve; BeaST, Brain Extraction based on nonlocal Segmentation Technique; CIT168, California Institute of Technology 168; DaT, Dopamine transport; TE, Echo time; FoV, Field of view; FSL, FMRIB Software Library; FLIRT, FMRIB's Linear Image Registration Tool; GRE, Gradient recalled echo; HC, Healthy control; LEDD, Levodopa equivalent daily dosage; MoCA, Montreal Cognitive Assessment; MDS, Movement Disorder Society; UPDRS-III, Unified Parkinson's Disease Rating Scale Motor Subscale; PD, Parkinson's disease; ppb, parts per billion; QSM, Quantitative susceptibility mapping; ROC, Receiver operating characteristic; RM-ANCOVA, Repeated measures analysis of covariance; TR, Repetition time; SNc, Substantia nigra pars compacta; SNr, Substantia nigra pars reticulata; T1w, T1-weighted; VTA, Ventral tegmental area.

* Corresponding author at: Department of Clinical Neurological Sciences, Western University, London, Ontario N6A 3K7, Canada.
E-mail address: penny.macdonald@gmail.com (P.A. MacDonald).

https://doi.org/10.1016/j.nicl.2024.103577
Received 7 August 2023; Received in revised form 19 December 2023; Accepted 7 February 2024
Available online 17 February 2024

This study highlights the importance of segmenting midbrain subregions, performed here using a standardized atlas, and demonstrates high accuracy of SNc iron measured with QSM at 3T MRI in identifying early PD patients. QSM measures of SNc show potential for inclusion in neuroimaging diagnostic biomarkers of early PD. An MRI diagnostic biomarker of PD would represent a significant clinical advance.

1. Introduction

Parkinson's disease (PD) is a progressive, neurodegenerative disorder, causing an array of motor and non-motor symptoms (Barone et al., 2009). Currently, there are no objective tests to diagnose or stage PD that are used in routine clinical practice (Mitchell et al., 2021). This aging-associated disorder is the fastest growing neurological disease in the world (Okunoye et al., 2022)Movement disorder neurologists are already outpaced at current PD prevalence, even ahead of the anticipated surge in cases, without commensurate training of new PD specialists (Miller and O'Callaghan, 2015; Ratliff et al., 2022). The availability of accurate and commonly-available diagnostic tests would improve clinical management, facilitating participation of generalists in managing this disease (Kim et al., 2019) Furthermore, this development is critical for advancing discovery of disease-modifying therapies and a cure for PD.

Early loss of dopaminergic neurons in the substantia nigra (SN) pars compacta (SNc) is widely accepted as the cause of motor deficits in PD (Ayton and Lei, 2014; Prasad et al., 2018). The N1 nigrosome is the first subregion within the SNc to degenerate (Perez Akly et al., 2019). In contrast, the SN pars reticulata (SNr) neurons are impacted non-specifically in later stages, potentially providing a negative control in early stages of PD (Hardman et al., 1996; McRitchie et al., 1996). Finally, the adjacent ventral tegmental area (VTA) underlies non-motor symptoms that develop in later stages of PD, with measures of this region potentially providing an index of PD progression (Alberico et al., 2015). Dissimilarities in degeneration of SNc, SNr, and VTA neuronal populations may arise from disparities in handling of calcium and iron, leading to differences in vulnerability to PD pathophysiology (Kubis et al., 2000; Lautenschläger et al., 2018; Moos and Morgan, 2004). Despite this understanding of the pathophysiology, there are currently no objective, diagnostic tests for PD that are sensitive, specific, and routinely accessible in clinical practice (Khan et al., 2019). Understanding the magnitude of this problem and the impact on patients, discovery of clinically useful biomarkers of PD is a highly active area of research (Peralta et al., 2022; Mitchell et al., 2021).

Although neuroimaging has revolutionized diagnosis and staging of many common neurological diseases, it currently plays a very limited role in the diagnosis of PD (Khan et al., 2019; Pyatigorskaya et al., 2018). The Neuroimaging Working Group of the International Parkinson and Movement Disorder Society (MDS) recently reviewed the literature on neuroimaging measures of PD (Peralta et al., 2022). They concluded that there is a need to achieve clearer normal versus pathological thresholds, superior performance in diagnosing early disease and tracking progression, as well as application of multimodal imaging approaches. Currently, the only approved imaging technique in clinical practice is dopamine transporter (DaT) imaging. A negative test greatly reduces the likelihood of idiopathic PD (Kim et al., 2019). DaT scanning has a number of disadvantages including its expense (McCleery et al., 2015), limited accessibility to clinicians, especially those who are operating outside of Movement Disorder clinics Peralta et al., 2022) as well as problems with tracking progression, and specificity of this measure in distinguishing PD from some of its neurodegenerative *mimics* (i.e., clinical conditions that resemble PD but have different pathophysiological mechanisms) (Kim et al., 2019; Ali and Morris, 2015). Furthermore, considering a review by Peralta and colleagues (2022), and another review of the PD biomarker literature by Mitchell and colleagues (2021), the mean PD disease duration of patient samples is ~ 4.5–5 years, with broad ranges, not ideal if a diagnostic measure is sought, and PD groups are typically $n \leq 30$–35. These are limitations of this literature given the research aims of developing a diagnostic test that will generalize to the clinical setting (Moos and Morgan, 2004). Once limitations present in this research, ours included, are resolved, prospective multicentred studies will be needed, testing the most promising biomarkers, optimally in combination, in much larger samples of early-staged PD patients relative to age-matched healthy controls (HCs) and PD mimics. Only then can these neuroimaging measures truly translate to clinical practice.

Acknowledging some of these limitations in the current study, the aim was to investigate the promise of imaging iron in midbrain subregions with MRI to distinguish and classify PD patients from HCs at the individual level. Due to the ubiquity of MRI, as well as the familiarity of clinicians with this modality, from general practitioners to subspecialists, we expect that MRI measures could be more easily integrated into routine non-specialist, clinical practice, where, unfortunately, PD patients will increasingly be managed given trends in PD prevalence that is not matched by training of new specialists (Sederman, 2022; Plouvier et al., 2017). Consequently, our overarching research programme aims to develop quantitative, reproducible, and automated MRI diagnostic and progression measures of PD.

Although iron is essential for cellular homeostasis and processes, it is also implicated in neurodegeneration (Pyatigorskaya et al., 2020). Hare and colleagues (2014) assessed vulnerability to oxidative stress in PD models through an iron-dopamine co-expression index (Hare et al., 2014). The SNc had a high iron-dopamine co-expression index suggesting greater vulnerability to oxidative stress, potentially explaining the resulting pattern of midbrain degeneration in PD. Dexter and colleagues (1991) found that total iron levels are elevated in the basal ganglia of PD patients using histology (Dexter et al., 1991). Nigral iron elevation is now increasingly recognized as an invariable feature of PD (Peralta et al., 2022). The properties of iron, its abundance in the midbrain, its involvement in oxidative stress and neurodegeneration, as well as findings of elevated iron in PD, make it an ideal candidate for detecting and tracking PD longitudinally (Ayton and Lei, 2014).

MRI can measure brain iron *in vivo* by assessing the impact of susceptibility on T2* relaxation times. Conventionally, R2* relaxometry has been used, however, its values can be dependent on orientation relative to the main magnetic field and other properties such as field strength (Sethi et al., 2019). Quantitative susceptibility mapping (QSM) is a newer technique that is less dependent on imaging parameters such as echo time (TE), field strength, and orientation, and thus could provide a more direct measure of susceptibility differences due to iron (Sethi et al., 2019; De Rochefort et al., 2010). QSM correlated well with iron content in deep gray matter nuclei, using histological measures such as Perls staining (Deistung et al., 2013; Deistung et al., 2017).

In some studies, QSM, indexing iron, is elevated in the total SN at the group level in PD patients compared to HCs, especially for later-staged PD patients (Sethi et al., 2019; Barbosa et al., 2015; Langkammer et al., 2016; Lotfipour et al., 2012). A useful biomarker must detect PD at the individual level (Du et al., 2016; Guan et al., 2017; Takahashi et al., 2018). Some studies noted elevated iron in PD patients in the SNc (Du et al., 2016; Guan et al., 2017; Takahashi et al., 2018) and in one study in the N1 nigrosome (Lancione et al., 2022). The use of manual segmentation in these studies causes a dependence on practitioners with neuroradiological expertise that could limit widespread adoption of these approaches. QSM values in the SN/SNc also correlated with clinical features of PD, including disease duration (Du et al., 2016; He et al., 2015), motor symptom severity (Langkammer et al., 2016; Wang et al.,

2016), cognitive symptom severity (Uchida et al., 2019; Uchida et al., 2020), and levodopa equivalent daily dosage (LEDD)—a measure of disease evolution and severity (Langkammer et al., 2016; Du et al., 2016). Iron in the SNr and VTA are often not investigated or reported. Though Zhang and colleagues (2023) aimed to assess QSM in the VTA, they opted for a combined measure of the dopamine-producing neurons in the VTA and the larger, adjacent, neuromelanin-containing but glutamatergic neurons in the parabrachial pigmented (PBP) nucleus, which is implicated in nociceptive pathways with unclear role in PD (Pauli et al., 2022; Pautrat et al., 2023). Taken together, these findings with iron imaging, and QSM specifically, in the total SN, the SNc and its subregions (i.e., N1 nigrosome), as well as VTA warrant further investigation for their potential to diagnose PD, and perhaps track progression.

Neuromelanin MRI has emerged as a proxy marker for midbrain dopamine neurons, though note that neuromelanin is not specific to dopamine-producing neurons, detected in other catecholamine-producing regions such as the locus coeruleus and, as previously-mentioned, in the PBP nucleus as well (Liu et al., 2023). Neuromelanin and iron are inversely related in the brain, and it is proposed that neuromelanin performs a regulatory function of iron, consisting of a dark pigment synthesized via iron-dependent oxidation of cytosolic catecholamines, including dopamine (Cassidy et al., 2019; Martínez et al., 2023). Using neuromelanin MRI, discrimination of PD patients and HCs has been achieved at the group-level and the single-subject level (Cassidy et al., 2019; Wang et al., 2023). Recent 3T MRI studies have explored both iron, using QSM, and neuromelanin, using neuromelanin MRI, in the SN in PD (Martínez et al., 2023; Jokar et al., 2023; Zhang et al., 2023). Jokar and colleagues (2023) found that QSM and neuromelanin measures in the SN, and the absence of the N1 nigrosome assessed by two raters with neuroradiology expertise, performed with comparable diagnostic accuracy in PD (i.e., 0.78, 0.75, and 0.78 respectively). Combining these measures, Jokar and colleagues distinguished PD patients from HCs with diagnostic accuracies above 0.90, sensitivity of 0.88, and specificity of 0.86–0.91. However, this study did not restrict to early PD (n = 100, disease duration 0.2–13 years), clinical information related to disease duration and severity were missing for some patients, and though the SN was segmented automatically, regions within SN were traced manually based on QSM and neuromelanin, overlain and using thresholding, a template, presumably the SNc was created and applied to PD. Finally, they did not use cross-validation approaches or an independent sample, to test whether their models, which were optimized to produce highest classification accuracy in their specific dataset, would generalize.

Martinez and colleagues (2023) also compared SNc QSM (diagnostic accuracy of 0.77) and neuromelanin (diagnostic accuracy of 0.86) and reported elevated iron in the lateral, medial-rostral, and caudal SNc for PD patients relative to HCs. Their idiopathic PD group ($n = 39$) had a lengthy disease duration of average 8.6 years (±0.9 SEM). Like Jokar and colleagues, their combined measures of QSM and neuromelanin in the SNc and other midbrain/pontine nuclei had highest diagnostic accuracies. Only logistic regression models that included iron and neuromelanin contrast ratios, as well as volumes, in the SNc, red nucleus, and locus coeruleus achieved AUCs above 0.90 in discriminating PD patients from HCs. Analysis in a small subgroup of 11 idiopathic PD patients ≤ 5 years disease duration (mean duration and range not reported), revealed QSM AUC = 0.71 and neuromelanin AUC = 0.81 both measured in SNc. As for the full group, combined measures performed best with an ROC-AUC above 0.90 for QSM and neuromelanin contrast ratios in the SNc, red nucleus, and locus coeruleus. Weaknesses of this study include the late-staged patients overall, the small early-staged PD sample, and the use of manual segmentation and identification of the ROIs by a neurologist in some steps and contrasts, despite automation of some aspects of ROI definition. More important, however, they do not report sensitivity and specificity, which makes it difficult to interpret their accuracies and the potential for these measures to generalize to the clinic. An advantage of Martinez and colleagues' study is that, though they did not test their models in an independent sample, which is the gold standard for assessing the generalizability of models, they did use bootstrapping × 1000 with replacement to improve the representativeness of their ultimate model.

We are not aware of any neuroimaging studies that have estimated iron in the SNc, SNr, total SN, and VTA separately in early-staged PD patients with 3T MRI using an atlas-based segmentation of midbrain nuclei. The latter is needed to ensure reproducibility of the approach across centres. Furthermore, to our knowledge, no investigations have assessed iron in VTA, in isolation, *in vivo* (Alberico et al., 2015). This has been due to the previous lack of atlases, the structure's small size, and insufficient contrast to properly evaluate VTA. The recently developed California Institute of Technology 168 (CIT168) probabilistic subcortical atlas includes the VTA and could be used to objectively outline this structure, as well as the SNc and SNr separately (Alberico et al., 2015; Pauli et al., 2018). Though neuromelanin appears to be an interesting and promising measure of PD, given differences between studies in sample characteristics, methods for extracting midbrain regions/subregions, statistical and modelling approaches, as well as infrequent direct statistical contrasts of models, to this point, the superiority of neuromelanin MRI or of MRI iron sequences in PD detection remains unclear (Martínez et al., 2023; Jokar et al., 2023; Zhang et al., 2023). Abnormal iron metabolism seems to precede neuromelanin changes in the SNc and striatum, both of which follow striatal dopaminergic denervation, according to findings by Biondetti and colleagues (2021). In light of this and given our interest in testing early-staged PD patients (mean disease duration = 2.40 ± 0.2 years), we opted to contrast two iron measures, QSM and R2*, in the current study. Furthermore, we will evaluate the potential of QSM versus R2* values in midbrain nuclei to distinguish early-staged PD patients from HCs at the group and single-subject levels. We will use ROC curve analyses for our single-subject level analyses and will directly compare diagnostic accuracy performance with the Hanley-McNeil method to remove any doubt about differences in potential of our iron measures in early PD.

Finally, we aimed to investigate whether 3T MRI performs comparably to 7T MRI. This sub-aim was proposed to investigate whether efforts to identify MRI biomarkers of PD have to this point been unsuccessful due to an insufficiency of imaging resolution. To our knowledge, this is the first time that the same early PD patients were tested with iron sequences at both 3T and 7T MRI field strengths to investigate changes in midbrain subregions in patients compared to HCs. If differences noted at 7T are also observed at 3T MRI, the possibility of diagnosing PD using MRI will be bolstered, given that 3T MRI is much more widely available, whereas 7T is relatively inaccessible.

2. Materials and methods

2.1. Participants

Twenty-two participants with PD and 23 age- and education-matched HCs participated in this experiment. All participants with PD were previously diagnosed by a licenced neurologist, had no co-existing diagnosis of dementia or another neurological or psychiatric disease, and met the UK Brain Bank criteria for the diagnosis of idiopathic PD (Hughes et al., 1992). All PD and no control participants were treated with dopaminergic therapy. Age- and education-matched controls were within five years of age and five years of education to the matched PD patient. Participants with PD were recruited through the movement disorders database at the London Health Sciences Centre. Participants abusing alcohol, prescription or illicit drugs, or taking cognitive-enhancing medications including donepezil, galantamine, rivastigmine, memantine, or methylphenidate were excluded. The Montreal Cognitive Assessment (MoCA) was performed on all participants to rule out cognitive impairment (Nasreddine et al., 2005). Due to a 7T MRI scanner upgrade, seven participants (two HCs and five PDs) only have

3T MRI data. Further, we excluded any participants who had a contra-indication to MRI.

The Movement Disorders' Society-Unified Parkinson Disease Rating Scale Part III (MDS-UPDRS-III) was scored by a licenced neurologist with sub-specialty training in movement disorders (P.A.M.) to assess the presence and severity of motor symptoms for all patients off dopaminergic medication (Martinez-Martin et al., 1997). Control participants were also screened to rule out undiagnosed neurological illness. Demographic and cognitive scores for all patients and controls were recorded (Table 1). UPDRS motor subscale scores off dopaminergic therapy, mean duration of PD, daily doses of dopamine replacement therapy in terms of levodopa equivalents, and motor deficit dominance was also recorded (Table 1). Calculation of LEDD for each patient was based on the theoretical equivalence to levodopa(mg) as follows: levodopa dose(mg) × 1 + levodopa controlled release(mg) × 0.75 + levodopa(mg) × 0.33 if on entacapone(mg) + amantadine(mg) × 0.5 + bromocriptine(mg) × 10 + cabergoline(mg) × 50 + pergolide(mg) × 100 + pramipexole(mg) × 67 + rasagiline(mg) × 100 + ropinirole(mg) × 16.67 + selegiline(mg) × 10 (Wüllner et al., 2010). All participants provided informed written consent to the protocol before beginning the experiment according to the Declaration of Helsinki. This study was approved by the Health Sciences Research Ethics Board of Western University.

3. MRI data acquisition

Participants were scanned once on a 3T Siemens MAGNETOM Prisma Fit whole-body scanner and once using an ultra-high field 7T Siemens MRI Plus MAGNETOM scanner at the Centre for Functional and Metabolic Mapping, Western University, Canada. A maximum of seven days was allowed between scans using a random counterbalanced design with respect to the scanning order. Each scanner had a 32-receiver channel head coil with head position fixation devices installed. On the 3T scanner, the standard body transmit coil was used, however on the 7T an 8-transmit channel radio frequency coil integrated in the receiver array was used for parallel transmit.

On the 3T scanner, a localizer image was obtained first to position participants. T1-weighted (T1w) anatomical scans were obtained for structural information, registration of quantitative maps and the segmentation of midbrain nuclei using the CIT168 probabilistic subcortical atlas (Pauli et al., 2018). T1w anatomical images were acquired using a magnetization-prepared rapid gradient echo (MPRAGE) sequence (repetition time (TR) = 2300 ms, echo time (TE) = 2.98 ms, flip angle = 9°, Field of View (FoV) = 256 × 256 mm^2, 159 slices, voxel size = 1 × 1 × 0.9 mm^3, receiver bandwidth = 160 Hz/Px, acquisition time = 5:35 min). High resolution GRE images (Deistung et al., 2008) were acquired with an rf-spoiled, flow compensated 3D gradient echo sequence with six echoes (TE 8.09 ms to 40.49 ms with an interval of 6.48 ms), and (TR = 52 ms, flip angle = 20°, FoV = 224 × 224 mm^2, 96 slices, voxel size = 0.5 × 0.5 × 2 mm^3, receiver bandwidth = 160 Hz/Px, acquisition time = 8:30 min).

On the 7T scanner, a localizer image was similarly obtained first to position participants. T1w images were acquired with a magnetization-prepared 2 rapid gradient echo (MP2RAGE) sequence (TR = 6000 ms, TE = 2.73 ms, flip $angle_1$ = 4°, flip $angle_2$ = 5°, FoV = 240 × 240 mm^2, 224 slices, voxel size = 0.7 × 0.7 × 0.7 mm^3, receiver bandwidth = 150 Hz/Px, acquisition time = 10:14 min). High resolution GRE images were acquired with an rf-spoiled, flow compensated 3D gradient echo sequence with four echoes (TE ranging from 4.61 ms to 15.50 ms and an equal interval of 3.63 ms), and (TR = 35 ms, flip angle = 13°, FoV = 220 × 220 mm^2, 128 slices, voxel size = 0.8 × 0.8 × 0.8 mm^3, receiver bandwidth = 310 Hz/Px, acquisition time = 9:07 min).

Table 1
Demographics and clinical information for participants.

Measure	3T MRI Cohort			7T MRI Cohort		
	HC (*n* = 23)	PD (*n* = 22)	*p*-value	HC (*n* = 21)	PD (*n* = 17)	*p*-value
Age, years	64.5 ± 1.0	67.1 ± 1.1	0.21	65.0 ± 1.5	67.8 ± 1.7	0.23
Sex, female: male	14: 9	8: 14	0.10	12: 9	6: 11	0.18
MoCA (out of 30)	28.3 ± 0.3	27.3 ± 0.4	0.15	28.1 ± 0.5	27.1 ± 0.7	0.17
MDS-UPDRS-III	0.7 ± 0.2	34.8 ± 2.3	< 0.001***	0.6 ± 0.3	39.4 ± 3.1	< 0.001***
Hoehn & Yahr	–	2 ± 0.1	–	–	2 ± 0.2	–
Disease Duration, years	–	2.4 ± 0.2	–	–	2.5 ± 0.4	–
Levodopa Equivalent Daily Dosage, mg	–	431 ± 38	–	–	394 ± 43	–
Motor Deficit Dominance, right: left	–	13: 9	–	–	13: 3	–

Means ± standard error mean reported. HC = healthy age-matched control; PD = Parkinson's disease; MoCA = Montreal Cognitive Assessment; MDS-UPDRS-III = Movement Disorder Society Unified Parkinson's Disease Rating Scale.
*** $P < 0.001$.

4. MRI data postprocessing

4.1. T1-weighted postprocessing

T1w image processing was performed using FMRIB Software Library (FSL) 5.0.11 (https://fsl.fmrib.ox.ac.uk/fsl/fslwiki/) (Jenkinson et al., 2012) and Advanced Normalization Tools (ANTs) 2.2 (https://picsl.upenn.edu/software/ants) (Avants et al., 2008). Brain Extraction based on nonlocal Segmentation Technique (BeaST) was used for skull-stripping T1w images from both 3T and 7T (https://github.com/khanlab/beast) (Eskildsen et al., 2012). Then bias fields for skull-stripped 3T and 7T T1w images were corrected using N4BiasFieldCorrection, followed by intensity normalization.

4.2. Gradient echo magnitude postprocessing

GRE magnitude images from all echoes were averaged then skull-stripped using BeaST. Skull-stripped averaged GRE magnitude images were then linearly registered to the final postprocessed T1w images using FMRIB's Linear Image Registration Tool (FLIRT).

4.3. QSM image generation

An in-house singular value decomposition algorithm based on Walsh et al. (2000) was employed to reconstruct the GRE raw data (Walsh et al., 2000; Klassen and Menon, 2013). This algorithm gives the least squares best estimate of the magnetization and avoids phase singularities. QSM processing was performed as follows: spatial phase unwrapping was accomplished using a 3D best path algorithm (Abdul-Rahman et al., 2007). The frequency at each voxel was then estimated by weighted least squares; each phase echo was weighted by the local signal-to-noise ratio in the corresponding T2*-weighted image. Finally, background removal and dipole inversion were performed simultaneously using a single-step QSM algorithm (Chatnuntawech et al., 2017). Since susceptibility values calculated by dipole inversion are relative, an offset was applied by forcing the mean value within the cerebrospinal fluid to be zero parts per billion (ppb).

Due to low contrast in QSM and R2* images, the transformation matrices from the earlier averaged GRE magnitude to T1w image registrations were used to perform linear registration of both quantitative maps onto T1w images using FLIRT. QSM images were then offset using

the mean susceptibility in the cerebrospinal fluid of each participant as an internal reference, which allows for between subject comparisons to be performed (Langkammer et al., 2012).

4.4. R2* relaxometry image generation

Non-linear least squares estimation of R2* was calculated at each voxel using the Levenberg–Marquardt algorithm (https://netlib.org/minpack/) (Marquardt, 1963; Levenberg, 1944) on the complex signal with code available at: (https://github.com/AlanKuurstra/qsm_sstv).

4.5. Atlas-based segmentation

The CIT168 probabilistic subcortical atlas was used for single atlas-based segmentation (https://neurovault.org/collections/3145/) (Pauli et al., 2018). This high-resolution atlas clearly demarcates the SNc, SNr, and VTA based on data from young controls in the Human Connectome Project database.

Pre-processed T1w images were registered with the MNI152N-lin2009cAsym template using an initial affine registration using block-matching, followed by deformable b-spline registration, both implemented in NiftyReg v1.3.9 (Modat et al., 2010; Modat et al., 2014). Overlay visualizations depicting the skull-stripping, affine registration, and deformable registration were generated for each subject to check for failures. Failures in affine registration were corrected by forcing initialization with an existing transformation matrix. Discrete and probabilistic segmentation images in the template spaces were automatically propagated to each participant's T1w space, using nearest neighbour interpolation for discrete segmentations, and linear for probabilistic segmentations. The boundaries of the midbrain nuclei: SNc, SNr, and VTA were based on these segmentations.

4.6. Statistical analysis

Demographic data for all participants was compared between groups using one-way ANOVA looking at Age, MoCA total scores, and MDS-UPDRS-III scores and a chi-square test was performed for Sex. For the three midbrain nuclei, PD patients were compared to controls for the mean susceptibility in parts per billion (ppb) in QSM images and mean R2* values (1/s) in R2* images for each brain hemisphere.

Separate 2 × 2 repeated measures analysis of covariance (RM-ANCOVA) was conducted with Group (PD versus HC) as the between-subjects factor and Hemisphere (Left versus Right) as the within-subjects variable, controlling for Age and Sex as covariates on a) QSM and b) R2* measures in the SNc, SNr, VTA, and total SN. These were performed separately for 3T and 7T MRI. Subcortical iron deposits increase with age and elderly males may display higher iron levels than elderly females, even when accounting for Age, thus warranting both as covariates for our analyses (Persson et al., 2015). For all statistical analyses, $p < 0.05$ was used as the statistical threshold. Benjamini-Hochberg correction was used to control the false discovery rate at $q = 0.05$ across all tests (Benjamini and Hochberg, 1995).

Mean ROC curve-area under the curve (AUC) were generated on *held-out data*, with repeated *k*-fold cross-validation, where repeat = 50 and $k = 5$, to assess the potential of our iron measures to discriminate PD patients from HCs at the single participant level (Table 2), using MATLAB (version R2018a, MathWorks, Natick, MA, USA). Mean susceptibility and R2* values were considered for both left and right hemispheres. The mean ROC-AUC was calculated to determine and compare diagnostic accuracy between techniques using the Hanley-McNeil method (Hanley and McNeil, 1983). A best cut-off point for sensitivity and specificity was determined using the Youden method. All statistical analyses were performed using IBM SPSS Statistics (version 25, IBM Corp., Armonk, NY, USA).

Table 2
Review of literature developing a PD diagnostic neuroimaging biomarker using structural MRI.

	Group-level Analysis Only	Classification Model without Testing in Independent Sample		Classification Model with Testing in Independent Sample	
		No cross-validation	Cross-validation	Single Centre	Multi-centred
PD vs. HC	Du et al. (2011) (MRI/DTI/R2*) Lotfipour et al. (2012) (QSM) He et al. (2015) (QSM/R2*) De et al. (2016) (SWI) Du et al. (2016) (QSM/R2*) Langkammer et al. (2016) (QSM/R2*) Peckham et al. (2016) (SWI) Acosta-Cabronero et al. (2017) (QSM) Guan et al. (2017) (QSM/R2*) Guan et al. (2017) (QSM/R2*) Xuan et al. (2017) (QSM) An et al. (2018) (QSM) Du et al. (2018) (QSM/R2*) Bergsland et al. (2018) (QSM) Chen et al. (2019) (QSM) Ghassaban et al. (2019) (QSM/R2*) Guan et al. (2019) (QSM/DTI) Sethi et al. (2019) (QSM) Uchida et al. (2019) (QSM) Ahmadi et al. (2020) (QSM/R2*) Sun et al. (2020) (QSM) Thomas et al. (2020) (QSM) Song et al. (2021) (QSM) Tan et al., 2021 (Tan et al., 2021) (QSM) Li et al. (2022) (QSM) Lee et al.	Barbosa et al. (2015) (QSM/R2*) Noh et al. (2015) (SWI)[d] Bae et al. (2016) (SWI)[e] Murakami et al. (2015) (QSM/R2*) Azuma et al. (2016) (QSM) Zhao et al. (2017) (QSM/R2*) Kim et al. (2018) (QSM) Sjöström et al. (2017) (QSM)[i] Takahashi et al. (2018) (QSM/NM) Takahashi et al. (2018) (QSM/NM) Li et al. (2019) (QSM/R2*) Azuma et al. (2019) (QSM) Shahmaei et al. (2019) (QSM) Meijer et al. (2015) (SWI)[f] He et al. (2021) (QSM)[g] Lee et al. (2021) (QSM) Tang et al. (2010) (PET/SPEHC)[a] Vaillancourt et al. (2009) (DTI)[b] Ohtsuka et al. (2014) (NM)[c] Jokar et al. (2023) (QSM/NM) Martinez et al. (2023) (QSM/NM) Zhang et al. (2023) (QSM/NM)	Present Study (QSM/R2*) Cheng et al. (2019) (QSM)	Xiao et al. (2021) (QSM)[h]	

(continued on next page)

Table 2 (*continued*)

	Group-level Analysis Only	Classification Model without Testing in Independent Sample		Classification Model with Testing in Independent Sample	
		No cross-validation	Cross-validation	Single Centre	Multi-centred
	(2000) (PET/SPEHC) Rolheiser et al. (2011) (DTI) Ofori et al. (2015) (DTI) Mak et al. (2015) (MRI) Biondetti et al. (2020) (NM) Schindlbeck et al. (2021) (PET/SPEHC) Zhou et al. (2021) (DTI)				
PD vs. mimic	Meijer et al. (2015) (SWI) Shimada et al. (2009) (PET/SPEHC)	Sjöström et al. (2017) (QSM)[i] Azuma et al. (2019) (QSM)		Chougar et al. (2021) (MRI)	Archer et al. (2019) (DTI)[j]

[a] Metabolic brain imaging identified PD (84% sensitivity, 97% specificity), MSA (85% sensitivity, 96% specificity), and PSP (88% sensitivity, 94% specificity).

[b] DTI of caudal SN distinguishes PD from HC with 100% AUC.

[c] NM-sensitive MRI differentiates PD, atypical parkinsonism, and HC.

[d] Abnormality in nigrosome 1 can be detected with 94.6% accuracy in PD patients.

[e] Sensitivity and specificity of detecting nigral hyperintensity in parkinsonism was 88.8% and 83.6% respectively. Concordance between MRI and PET imaging was 86.2%.

[f] MR-imaging had specificity of 80–90% but sensitivity of 50–80% for detecting atypical parkinsonism. AUC increased from 0.75 to 0.83 for identifying MSA-P, and from 0.76 to 0.82 for identifying atypical parkinsonism as a whole.

[g] Semi-automated system not independently validated. AUC for different models created ranged from 0.965 to 0.983.

[h] Independent testing consisted of created model with 80% of participants and tested on remaining 20%. Accuracy was 86%.

[i] PD distinguished from PSP with ROC of 0.97.

[j] Independent testing consisted of created model with 80% of participants and tested on remaining 20%. Automated imaging was used to differentiate parkinsonism but not parkinsonism vs HC.

5. Results

5.1. Demographics

Our early-stage PD patients and HCs did not differ significantly in Age, Sex, or cognitive ability, the latter measured using MoCA Total Scores (Table 1). In our 3T MRI cohort, early-stage PD patients had a mean disease duration of 2.40 ± 0.2 years and a Hoehn & Yahr score of 2 ± 0.1 (Hoehn and Yahr, 1967; Goetz et al., 2004). For 7T, early-stage PD patients had a mean disease duration of 2.50 ± 0.4 years and a Hoehn & Yahr score of 2 ± 0.2. Recall that seven participants did not participate in the 7T scans due to a scanner upgrade. The mean MDS-UPDRS-III (i.e., the motor sub-scale) score for PD patients was 34.8 ± 2.3 in the 3T cohort and 39.4 ± 3.1 in the 7T cohort (Goetz et al., 2008). These data for PD patients and HCs are presented in Table 1. As expected, PD patients had statistically higher scores on the MDS-UPDRS-III ($t = 13.9$, $p < 0.0001$).

5.2. Iron imaging at 3T and 7T MRI

Separate 2 × 2 RM-ANCOVAs were performed at 3T and 7T MRI for QSM and R2* relaxometry to assess the group-level differences between PD patients and HCs in the SNc, SN, SNr, and VTA. Group was the between-subjects factor, and Hemisphere as the within-subjects variable. Age and Sex were covariates.

5.3. QSM in the SNc

For QSM values in the SNc at 3T and 7T MRI, there were significant main effects of Group [$F(1,41) = 17.4$, $mSe = 3123$, $p_{adj} = 0.001$ at 3T; $F(1,31) = 11.1$, $mSe = 1830$, $p_{adj} = 0.01$ at 7T], revealing higher mean susceptibility for PD patients than HCs (Fig. 2A and B). There were no significant main effects of Hemisphere [$F(1,41) = 2.29$, $mSe = 984$, $p_{adj} = 0.31$ a 3T; $F(1,31) < 1$ at 7T] nor significant Group × Hemisphere interactions [$F(1,41) < 1$ at 3T; $F(1,31) < 1$ at 7T].

5.4. R2* in the SNc

For R2* values in the SNc, the main effect of Group was not significant at 3T [$F(1,41) = 2.82$, $mSe = 92$, $p_{adj} = 0.96$; Fig. 3A] but was marginally significant at 7T [$F(1,31) = 7.47$, $mSe = 148$, $p_{adj} = 0.052$; Fig. 3B]. The latter reflected marginally higher R2* values for the PD group. No main effects of Hemisphere [$F(1,41) < 1$ at 3T; $F(1,31) < 1$ at 7T], nor Group × Hemisphere interactions [$F(1,41) = 6.66$, $mSe = 23$, $p_{adj} = 0.06$ at 3T; $F(1,31) < 1$ at 7T] were significant.

5.5. QSM in the SNr

There were no significant main effects of Group or Hemisphere, nor Group × Hemisphere interactions for QSM values in the SNr [$F(1,41) < 1$ at 3T for all; $F(1,31) < 1$ at 7T for all]. See Fig. 4A for results from 3T MRI analyses.

5.6. R2* in the SNr

The main effects of Group [$F(1,41) < 1$ at 3T; $F(1,31) = 2.07$, $mSe = 244$, $p_{adj} = 0.46$ at 7T] and Hemisphere [$F(1,41) < 1$ at 3T; $F(1,31) < 1$ at 7T], and the Group × Hemisphere interactions [$F(1,41) = 3.47$, $mSe = 26$, $p_{adj} = 0.96$ at 3T; $F(1,31) < 1$ at 7T] on R2* values in the SNr were not significant.

5.7. QSM in the SN

For QSM values in the SN, there were no significant main effects of Group [$F(1,41) = 2.3$, $mSe = 974$, $p_{adj} = 0.30$ at 3T; $F(1,31) = 3.6$, $mSe = 914$, $p_{adj} = 0.12$ at 7T]. There were no significant main effects of Hemisphere [$F(1,41) = 2.73$, $MSe = 901$, $p_{adj} = 0.28$ at 3T; $F(1,31) < 1$ at 7T] nor significant Group × Hemisphere interactions [$F(1,41) < 1$ at 3T; $F(1,31) < 1$ at 7T].

5.8. R2* in the SN

For R2* values in the SN, there were no significant main effects of Group [$F(1,41) < 1$ at 3T; $F(1,31) < 1$ at 7T]. There were no significant main effects of Hemisphere [$F(1,41) < 1$ at 3T; $F(1,31) < 1$ at 7T] nor significant Group × Hemisphere interactions [$F(1,41) < 1$ at 3T; $F(1,31) < 1$ at 7T].

5.9. QSM in the VTA

We found no significant main effects of Group [$F(1,41) = 3.20$, $mSe = 348$, $p_{adj} = 0.15$ at 3T; $F(1,31) < 1$ at 7T] or Hemisphere [$F(1,41) = 1.48$, $mSe = 514$, $p_{adj} = 0.42$ at 3T; $F(1,31) = 2.68$, $mSe = 149$, $p_{adj} = 0.36$ at 7T], nor significant Hemisphere × Group interactions [$F(1,41) =$

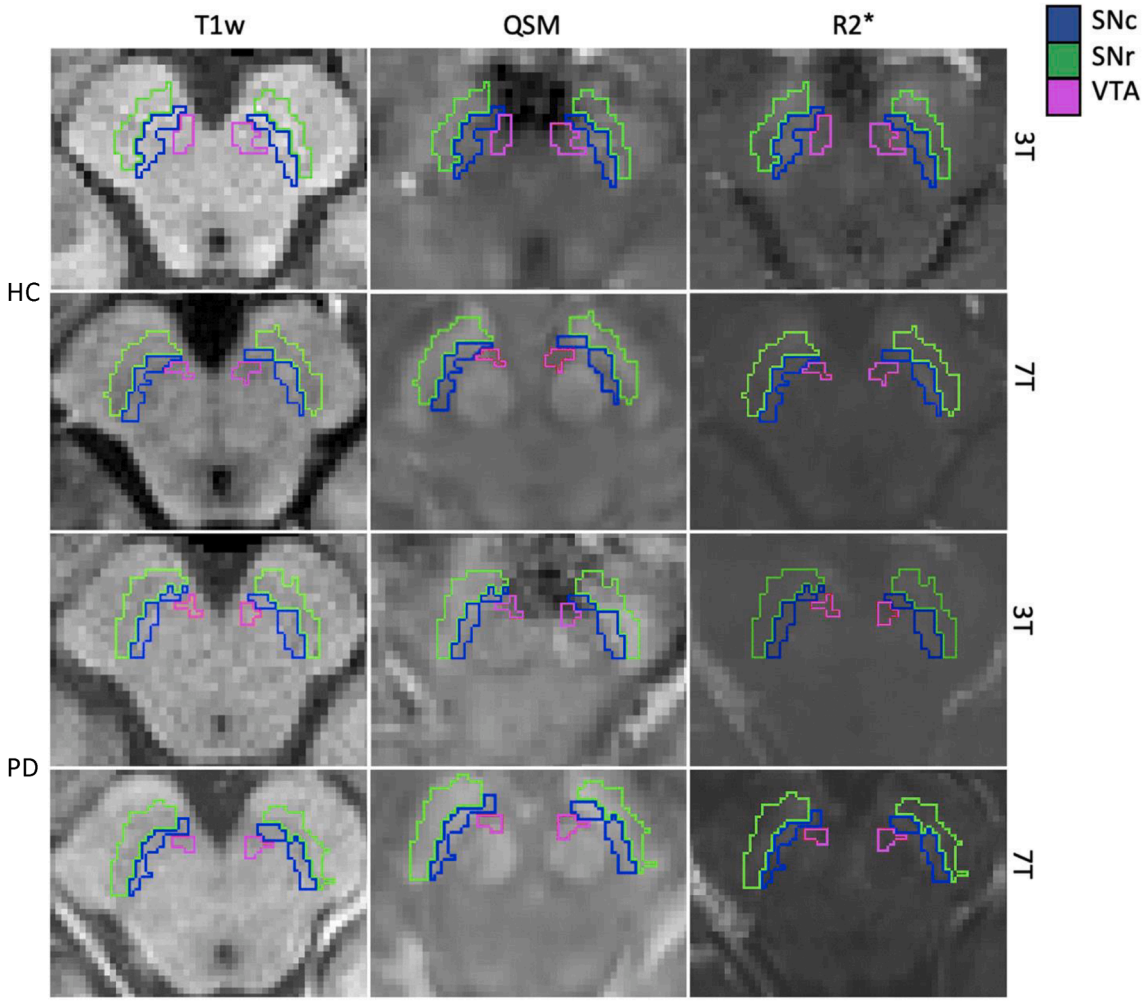

Fig. 1. Example segmentation of midbrain nuclei on T1w, QSM, and R2* maps of an age-matched healthy control and an early-stage PD patient. Top row shows the healthy control (HC) substantia nigra pars compacta (SNc), substantia nigra pars reticulata (SNr), and ventral tegmental area (VTA) from CIT168 atlas mapped onto 3-Tesla (T) images in the axial plane: T1-weighted (T1w), QSM, and R2* relaxometry. Second row shows the same HC at 7T. Third row shows early-stage PD midbrain nuclei mapped onto 3T images in the axial plane. Bottom row shows the same PD patient at 7T. The SNc is shown in blue, SNr in green, and VTA in magenta for all images. (For interpretation of the references to colour in this figure legend, the reader is referred to the web version of this article.)

3.20, $mSe = 1111$, $p_{adj} = 0.24$ at 3T; $F(1,31) < 1$ at 7T] on QSM values in the VTA (Fig. 4B).

5.10. R2* in the VTA

There were no significant main effects of Group [$F(1,41) = 1.62$, $mSe = 125$, $p_{adj} = 0.53$ at 3T; $F(1,31) < 1$ at 7T] or Hemisphere [$F(1,41) < 1$ at 3T; $F(1,31) < 1$ at 7T], and no significant Hemisphere × Group interactions [$F(1,41) = 7.12$, $mSe = 19$, $p_{adj} = 0.06$ at 3T; $F(1,31) = 1.42$, $mSe = 19$, $p_{adj} = 0.57$ at 7T] in R2* values in the VTA.

5.11. ROC curve analyses in the SNc

Looking at SNc mean susceptibility from QSM at 3T, the mean AUC was 0.83 (SEM = 0.0036, 95 % CI = 0.82–0.84, $p < 0.001$) with a sensitivity of 0.76 and specificity of 0.77 using the Youden index criteria (Fig. 5A). For QSM at 7T, the mean AUC was 0.80 (SEM = 0.0037, 95 % CI = 0.79–0.81, $p < 0.001$) with a sensitivity of 0.70 and a specificity of 0.77 (Fig. 5B).

For comparison, the ROC curves for QSM values of the SNr, total SN, and VTA at 3T are shown in Fig. 5C–E. Mean AUCs of 0.44 and 0.40 for SNr and SN revealed poor performance. Mean AUC of 0.68 for the VTA revealed fair performance.

For SNc mean R2* value from R2* relaxometry at 3T, the mean AUC was 0.54 (SEM = 0.0098, 95 % CI = 0.51–0.56, $p = 0.62$) with a sensitivity of 0.60 and a specificity of 0.49 using the Youden index (Fig. 6A). For R2* at 7T, the mean AUC was 0.74 (SEM = 0.0077, 95 % CI = 0.72–0.76, $p = 0.002$) with a sensitivity of 0.56 and a specificity of 0.69 (Fig. 6B).

QSM revealed higher mean AUC than R2* relaxometry at 3T ($Z = 2.71$, $p = 0.007$), but not at 7T ($Z = 0.51$, $p = 0.61$), using the Hanley-McNeil method, suggesting that QSM values in SNc have higher diagnostic accuracy for early-staged PD than R2* at 3T MRI, but not at 7T. Using the Hanley-McNeil method, we found no significant differences in mean AUC between field strengths (i.e., 3T vs 7T MRI) for QSM ($Z = 0.30$, $p = 0.76$) or R2* ($Z = 1.62$, $p = 0.10$) (Hanley and McNeil, 1983).

6. Discussion

The overarching aim of this study was to investigate potential MRI biomarkers of early-staged PD (mean disease duration = 2.40 ± 0.2 years). We imaged iron levels in midbrain nuclei and their subregions that are differentially affected by PD, using two a) quantitative techniques and b) MRI field strengths (Dexter et al., 1991; Sethi et al., 2019). Furthermore, the SNc, SNr, total SN, and VTA were segmented using objective, atlas-based methods that are entirely reproducible. In keeping

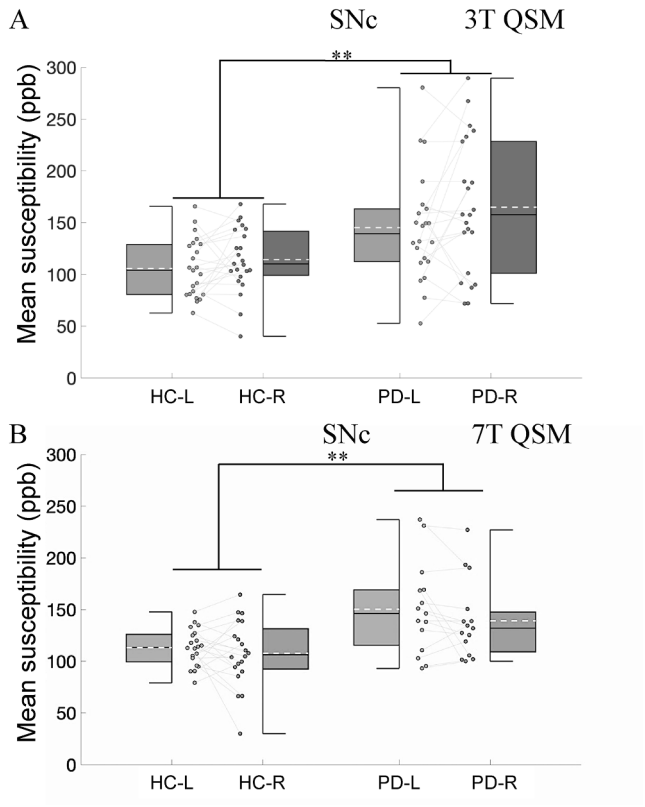

Fig. 2. Mean susceptibility for the SNc of early-stage PD patients and age-matched healthy controls in MRI acquired at 3T and 7T. Data show paired hemispheric means (-L for left and -R for right) for all participants in scatterplots with corresponding boxplots demonstrating median and interquartile range in black lines. Substantia nigra pars compacta (SNc) mean susceptibility in ppb from quantitative susceptibility mapping (QSM) at both field strengths are shown as dashed white lines. Significant group differences were found using RM-ANCOVA on data from 3T, $F(1,41) = 17.4$, $p_{adj} = 0.001$, and 7T MRI, $F(1,31) = 11.1$, $p_{adj} = 0.01$, with PD patients showing increased iron deposition. 3T: $n_{HC} = 23$, $n_{PD} = 22$, 7T: $n_{HC} = 20$, $n_{PD} = 15$. ** $p_{adj} \leq 0.01$.

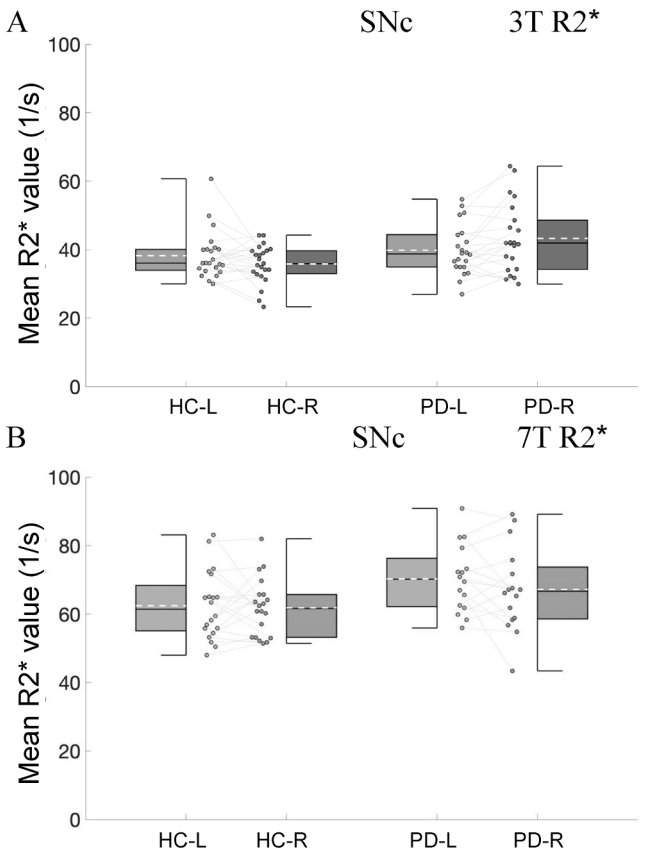

Fig. 3. Mean R2* values for the SNc of early-stage PD patients and age-matched healthy controls at 3T and 7T. Data show paired hemispheric means (-L for left and -R for right) for all participants in scatterplots with corresponding boxplots demonstrating median and interquartile range in black lines. SNc mean R2* values in 1/s from R2* at both field strengths are shown as dashed white lines. Using RM-ANCOVA, marginally significant differences were found between groups at 7T, $F(1,31) = 7.47$, $p_{adj} = 0.052$, with PD patients showing increased iron deposition. 3T: $n_{HC} = 23$, $n_{PD} = 22$, 7T: $n_{HC} = 20$, $n_{PD} = 15$.

with our predictions that are informed by studies of PD pathophysiology (Moos and Morgan, 2004; Pyatigorskaya et al., 2018), early-staged PD patients had significantly elevated QSM values in the SNc, indexing higher iron levels, compared to age-matched HCs at both 3T and 7T MRI. PD patients also displayed marginally increased R2* values in the SNc, our second measure of iron, but only at 7T MRI. In contrast, there were no significant differences in QSM or R2* values between early-staged PD patients and HCs at the group level when looking at the SNr, total SN, and VTA. The findings in the SNr and VTA were expected, given the early-stage of our patients, and provided negative controls for our SNc results.

ROC curve analyses using QSM values in the SNc revealed good diagnostic accuracy in discriminating early-staged PD (mean disease duration = 2.40 ± 0.2 years) from HCs with mean AUC = 0.83 (95 % CI = 0.82–0.84), sensitivity = 0.76, and specificity = 0.77 at 3T and mean AUC = 0.80 (95 % CI = 0.79–0.81), sensitivity = 0.70, and specificity = 0.77 at 7T (Fig. 4A and 4B). In contrast, ROC curve analyses using R2* values in SNc performed poorly, near chance in distinguishing PD and HCs at the single-subject level (Fig. 5). The mean AUC using QSM values in SNc was statistically better than the mean AUC using R2* values in SNc at 3T using the Hanley-McNeil method. Not surprisingly, given that there were no group-level differences, neither iron measure in the SNr, total SN, and VTA successfully classified PD patients from HCs at the individual level. Finally, our AUCs for QSM in the SNc discriminating PD and HCs were statistically equivalent at 3T and 7T MRI, using the Hanley-McNeil method. This absence of difference is not evidence of equivalence, given that the probability of falsely failing to reject the null hypothesis is not set by the experimenter, in contrast to the Type I error rate, and the determinants are not controlled. For examples of potential causes of our findings, there were fewer participants scanned at 7T MRI and the use of a 7T atlas might have proved more sensitive. Nonetheless, our results did not provide evidence that 7T was, in fact, superior.

Contrasting measures of iron and neuromelanin in the diagnosis of PD.

QSM outperformed R2* relaxometry in classifying early PD patients relative to HCs at the single-subject level. This is in line with previous studies that have found that QSM is more sensitive to iron levels in PD than R2* relaxometry (Pyatigorskaya et al., 2018; Ravanfar et al., 2021). Others have investigated neuromelanin as a PD biomarker. Neuromelanin is inversely related to iron levels in midbrain and pontine (i.e., locus coeruleus) structures that are implicated in PD. Wang and colleagues (2023) measured neuromelanin in the total SN, outlined using manual tracing, in later-staged PD patients ($n = 64$; disease duration = 5.35 ± 3.05 years; $n = 32$ had Freezing of Gait;) relative to HCs ($n = 32$) (Wang et al., 2023). Fitting an ROC curve to their training dataset, not relative to a hold-out or entirely independent test set, they achieved AUC = 0.87, distinguishing PD patients for HCs in their data. Jokar and colleagues (2023) and Martinez and colleagues (2023) measured both QSM and neuromelanin in PD. Jokar and colleagues attained comparable PD diagnostic accuracy using QSM and neuromelanin in the SNc (AUC = 0.78 and 0.75 respectively) in a PD sample who ranged broadly

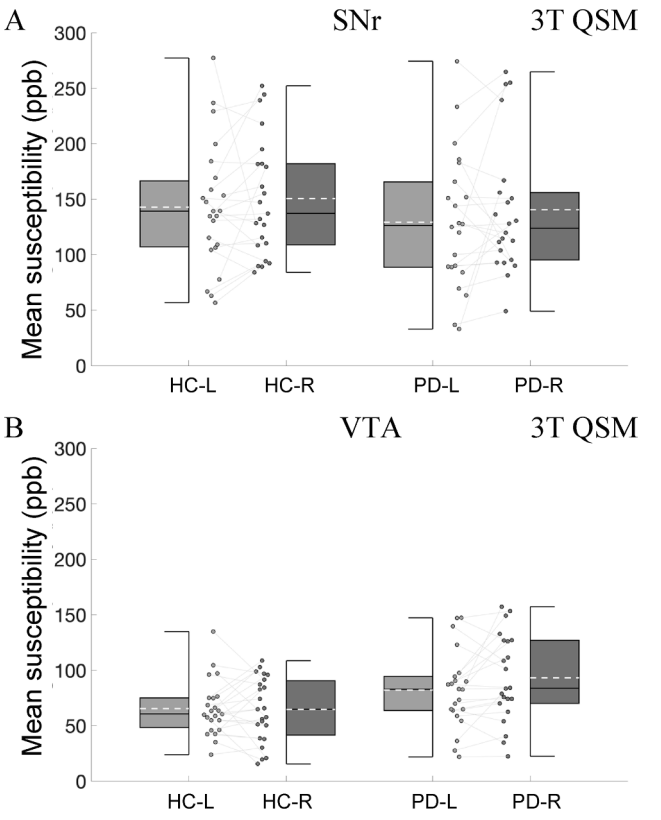

Fig. 4. Mean susceptibility for the SNr and VTA of early-stage PD patients and age-matched healthy controls at 3T. Data show paired hemispheric means (-L for left and -R for right) for all participants in scatterplots with corresponding boxplots demonstrating median and interquartile range in black lines. Substantia nigra pars reticulata (SNr) (A) and ventral tegmental area (VTA) (B) mean susceptibilities in ppb from QSM at 3T are shown as dashed white lines. Using RM-ANCOVA, no significant group differences were found between PD patients and controls in the SNr, $F(1,41) < 1$, or VTA, $F(1,41) = 3.2$, $p_{adj} = 0.15$. 3T: $n_{HC} = 23$, $n_{PD} = 22$.

in disease duration (i.e., 0.2–13 years). Martinez and colleagues reported lower AUC = 0.77 and 0.71 for QSM compared to AUC = 0.86 and 0.81 for neuromelanin in their total sample ($n = 39$; disease duration 2–23 years) and small sample of early-staged idiopathic PD patients ($n = 11$; mean and range not reported but all ≤ 5 years) respectively (Martínez et al., 2023). They did not confirm that these AUC differences were statistically significant, though this seems possible. Determining whether neuromelanin is superior to QSM/iron as a diagnostic measure of PD remains fraught given significant methodological differences across studies and controversy between studies that contrasted both measures within the same patients. Investigations by Biondetti and colleagues (2021), suggesting that iron elevation in the SNc precede reductions in neuromelanin (Martínez et al., 2023; Biondetti et al., 2021), add the important caveat that stage of disease might also impact this issue. In our study, we found good diagnostic accuracy of PD patients versus HCs, with SNc iron, potentially because we investigated early-staged PD patients (mean disease duration = 2.40 ± 0.2 years).

There are many differences between studies reported in the literature that hamper direct comparisons of the diagnostic measures conveyed (Table 2). In our study, we report classification accuracies using QSM values in the SNc (mean AUC = 0.83, 95 % CI = 0.82–0.84 at 3T and mean AUC = 0.80, 95 % CI = 0.79–0.81 at 7T) that refer to PD-HCs mean discrimination accuracy a) of the tests of the model in the hold-out set, using repeated cross-validation and b) not for fitting the model to training data as others report (Jokar et al., 2023; Wang et al., 2023), or c) using bootstrapping with resampling techniques that increase the representativeness of the model (Martínez et al., 2023). Assessing true generalizability requires testing diagnostic models in an entirely independent sample, which none of the studies reported here, ours included, have achieved to this point. Nonetheless, to increase the generalizability of our findings, we tested at two field strengths, employed QSM and R2* techniques, and used repeated *k*-folds cross-validation on our limited data to enhance the likelihood our ROC findings will replicate. These methodological differences alone preclude direct contrasts of measures across studies. Furthermore, in our study, we use a reproducible, atlas-based segmentation of midbrain structures and subregions on these structures. Most other studies employ manual segmentations of midbrain nuclei or subregions at some stage in their process (e.g., SNc) (Martínez et al., 2023; Barbosa et al., 2015; Ariz et al., 2023). Segmentation of structures by individuals with particular expertise, such as neuroscientists, neurologists, or neuroradiologists, might provide more precise identification of structures, yielding greater sensitivity, though reliance on a skilled individual to perform the segmentation hampers exporting the method, and risks variability across centres. Finally, in our study, we specifically recruited early-staged PD patients (mean disease duration = 2.40 ± 0.2 years), compared to samples with mean disease duration of 8.6 ± 5.4 years in Martinez et al. (2023) and 4.85 ± 2.7 years in Zhang et al. (2023), as well as with a range of 0.2–13 years disease duration in Jokar et al. (2023). Taken together, these differences in this literature constrain direct comparisons between measures, as well as extrapolation of findings and interpretation beyond the specific conditions of individual studies to this point, given lack of validation. To fully understand the potential of QSM and neuromelanin separately or combined as diagnostic measures in PD, future studies should collect these measures in the same, much larger, early-staged PD patients, with similar methods, and evaluating statistical differences between AUCs achieved in independent test sets (e.g., using the Hanley-McNeil method). Based on previous studies, it is likely that highest diagnostic accuracies will be accomplished by combining QSM and neuromelanin, though understanding the strengths and weaknesses of each measure, at different stages of disease and in PD subgroups remains an important endeavour.

Isolating midbrain subregions improves diagnosis of PD and estimation of progression

A specific aim of this study was to investigate whether segmenting and isolating midbrain structures that are differentially implicated in early PD would improve the sensitivity of QSM or R2* to detect changes that are known to occur even in early PD (Barbosa et al., 2015; Guan et al., 2017). Iron values in the total SN (i.e., SNc and SNr combined), revealed no significant group differences (Supplementary Fig. 1), nor an ability to distinguish individual PD patients from HCs (Fig. 4D) (Peralta et al., 2022; Sederman, 2022; Hare et al., 2014; Deistung et al., 2008). This is in line with previous studies that reveal measures of iron from total SN nigra are relatively insensitive to pathophysiological changes in early-staged PD (Barbosa et al., 2015; He et al., 2015). This is potentially because the SNr seems relatively impervious to iron accumulation, in early PD[78,80,] and consistent with this concept, we found no group-level, PD-HCs difference in the SNr in our early-staged PD. There is some evidence that QSM increases in SNr in late PD (Chen et al., 2019). In light of this, it seems imperative to isolate the SNc or perhaps even subregions of SNc to derive the most sensitive and accurate MRI diagnostic biomarkers of early-staged PD.

QSM and R2* measures of SNr and VTA had no ability to discriminate our PD patients and HCs (Fig. 4C and 4E). This was expected given our understanding of PD pathophysiology and previous findings, though measures from these regions might be helpful in tracking PD progression (Sethi et al., 2019; Barbosa et al., 2015; Du et al., 2016; Guan et al., 2017). In segmenting the SN/VTA, we provide an *in vivo* assessment of iron in human VTA. Previous segmentation algorithms have had difficulty delineating the subtle border between the SNc and SNr, let alone providing reliable boundaries of the much smaller VTA (Pauli et al., 2018; Eapen et al., 2011). This is complicated by the lack of consensus in

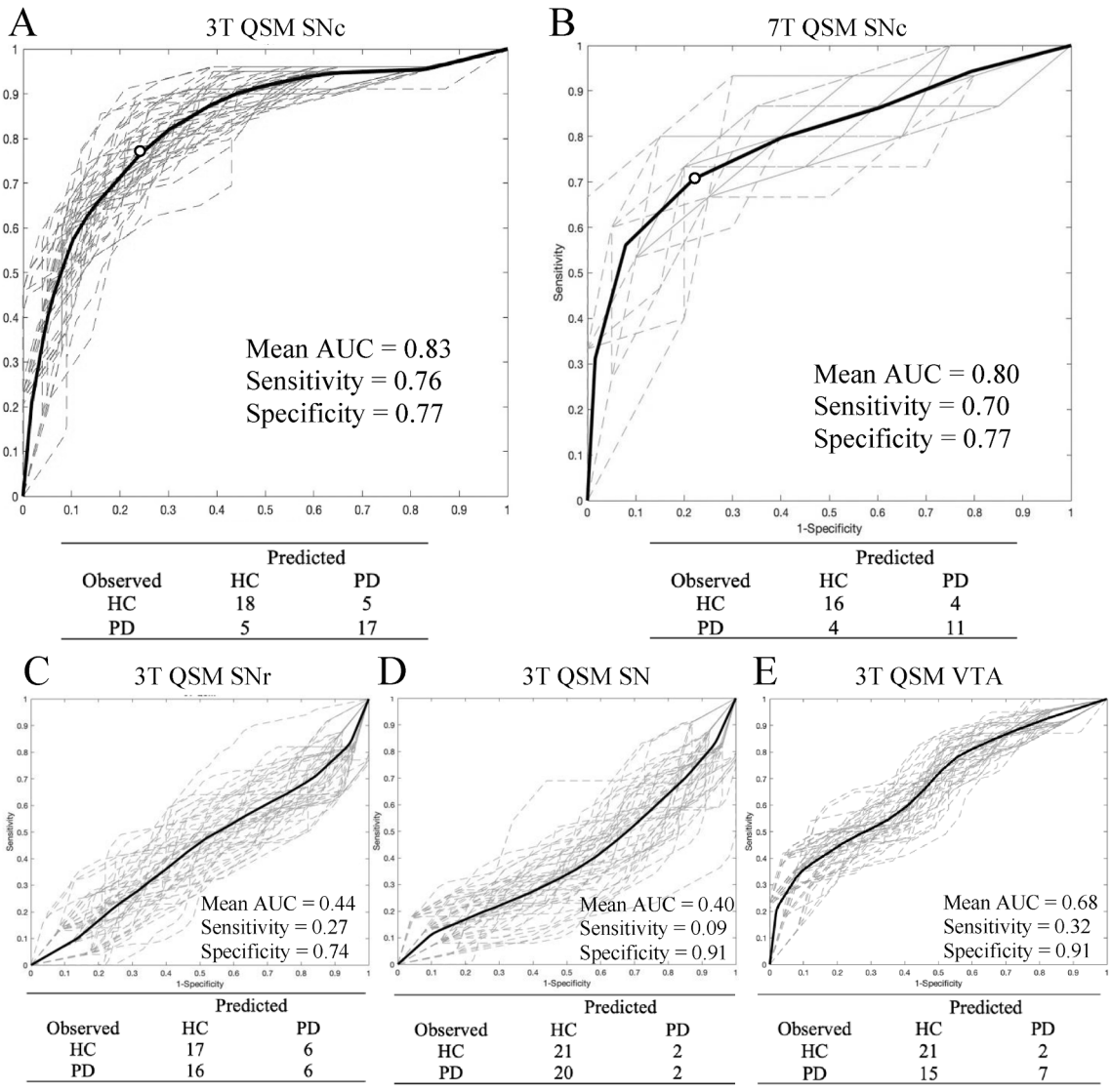

Fig. 5. ROC curves for SNc, SNr, SN, and VTA mean susceptibility at 3T and SNc mean susceptibit7T with SNr, whole SN, and VTA mean susceptibility at 3T. Data show confusion matrices and ROC curves for 50 repeated 5-folds cross-validation (dash lines) and average ROC curve (black line) for QSM at 3T in the SNc (A), QSM at 7T in the SNc (B), QSM at 3T in the SNr (C), SN (D), and VTA (E) of early-stage PD patients versus controls. 3T SNc: Mean AUC = 0.83 (95 % CI = 0.82–0.84), n_{HC} = 23, n_{PD} = 22, 7T SNc: Mean AUC = 0.80 (95 % CI = 0.79–0.81), n_{HC} = 20, n_{PD} = 15, 3T SNr: Mean AUC = 0.44 (95 % CI = 0.40–0.48), n_{HC} = 23, n_{PD} = 22, 3T SN: Mean AUC = 0.40 (95 % CI = 0.36–0.44), n_{HC} = 23, n_{PD} = 22, 3T VTA: Mean AUC = 0.68 (95 % CI = 0.65–0.71), n_{HC} = 23, n_{PD} = 22.

the literature about the anatomical nomenclature to describe the VTA (Trutti et al., 2019). Similar challenges present themselves when defining SNc, from SN and further from the N1 nigrosome subregions that are challenges we and others are tackling (Takahashi et al., 2018). Atlas-based or automated segmentation approaches are expected to overcome these issues, allowing for reproducibility across sites. This is an essential feature of a clinically useful neuroimaging biomarker of PD (Trutti et al., 2019). Estimates of iron using QSM and R2* were not different between our groups in the VTA even at 7T MRI. However, we anticipate that VTA iron, like SNr iron, might serve as a potential progression biomarker, given that VTA and SNr degenerates later than SNc. Investigations in mid-staged and late-staged PD patients, preferably followed longitudinally, could confirm this. Work by Zhang and colleagues (2023) has shown that after Hoehn & Yahr Stage 2, PD patients (n = 101, disease duration 4.9 years) show bilateral VTA iron elevation in comparison to HCs, however their inclusion of the PBP nucleus is potentially confounding and they did not distinguish across different disease stages to see if magnitude of QSM correlates with measures of PD progression/severity or other PD symptoms/subtypes (Zhang et al., 2023).

Measures of the ventrolateral subregion of the SNc, the N1 nigrosome, the region first degenerated in PD (Kish et al., 1988; Huddleston et al., 2017), have shown promise as biomarkers (Jokar et al., 2023; Ariz et al., 2023; Chau et al., 2020; Mahlknecht et al., 2017). Diagnostic accuracies, sensitivities, and specificities range widely (Jokar et al., 2023; Ariz et al., 2023; Prasuhn et al., 2021), however, and sample sizes in these studies are generally small ($n \langle 100$), with few studies focussing exclusively on early PD, and methodologies ranging from visual inspection by expert neuroradiologists (Prasuhn et al., 2021), quantitative measures such as iron or neuromelanin extracted from hand-drawn subregions (Kim et al., 2019; Barbosa et al., 2015), to studies that have sought to automate the location of the N1 nigrosome based on healthy control templates (Martínez et al., 2023; Ariz et al., 2023). When directly contrasted in the same studies, measures of iron or neuromelanin in the total SNc and the N1 nigrosome subregion have generally not shown a clear advantage one relative to the other (Jokar et al., 2023; Ariz et al., 2023). In all cases, models that combine measures of iron and neuromelanin, from SNc and N1 nigrosome, perform with highest

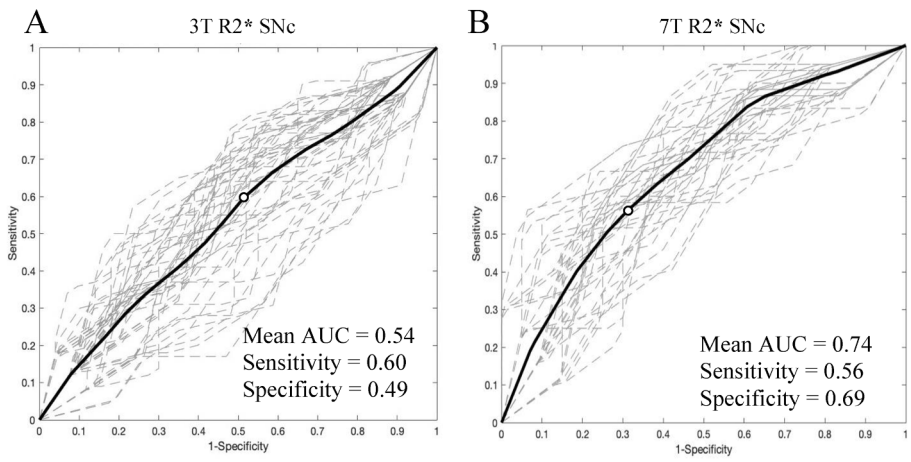

	Predicted	
Observed	HC	PD
HC	12	11
PD	9	13

	Predicted	
Observed	HC	PD
HC	14	6
PD	6	9

Fig. 6. ROC curves for SNc mean R2* value at 3T and 7T. Data show ROC curves for 50 repeated 5-folds cross-validation (dash lines) and the average ROC curve (black line) for R2* in the SNc of early-stage PD patients versus controls. 3T: Mean AUC = 0.54 (95 % CI = 0.51–0.56, $p = 0.62$), $n_{HC} = 23$, $n_{PD} = 22$, 7T: Mean AUC = 0.74 (95 % CI = 0.72–0.76, $p = 0.002$), $n_{HC} = 20$, $n_{PD} = 15$.

accuracy (Martínez et al., 2023; Jokar et al., 2023; Ariz et al., 2023). The N1 nigrosome has shown limited potential to measure progression of PD, possibly related to significant degeneration at the time of PD diagnosis (Wang et al., 2017). Finally, the N1 nigrosome lacks specificity for PD relative to other forms of Parkinsonism (Wang et al., 2017; He et al., 2023; Shams et al., 2017).

MRI diagnostic measures in current clinical context.

Despite limitations of our study, chief among them the unlikelihood that a single MRI measure will be sufficiently sensitive and specific to reliably diagnose PD—a complex, heterogeneous, and progressive disease, we present a *quantitative* neuroimaging biomarker using QSM as a measure of iron in SNc that distinguishes early-staged PD patients (mean disease duration = 2.40 ± 0.2 years) and HCs at the single-subject level, with AUC = 0.83, sensitivity = 0.76, specificity = 0.77. Furthermore, our results suggest that 3T MRI resolution is sufficient. Based on these findings, as well as those from other recent studies of iron or neuromelanin in midbrain (Martínez et al., 2023; Jokar et al., 2023; Zhang et al., 2023; Chougar et al., 2022; Biondetti et al., 2020) or striatal (Alushaj et al., 2023) subregions, there is optimism that neuroimaging-based diagnostic measures of PD will be achievable in the near future, to fill the anticipated gap in PD management (Ou et al., 1990).

For context, the clinical diagnostic accuracy in an early-stage PD cohort followed for five years was 91.5 % for movement disorder experts and 84 % for general neurologists and geriatricians in a study conducted at the National Hospital for Neurology and Neurosurgery (Queens Square, UK) (Virameteekul et al., 2023). Although our single MRI measure falls short of the accuracy of experts in movement disorders, should it replication and generalize, it paralleled the performance of neurologists and geriatricians in this study at a premier centre focused on Neurology and Neurosurgery. Though performance of all clinicians in this study improved beyond the accuracy of our measure when they referred to the MDS PD clinical diagnostic guidelines (Postuma et al., 2015), these guidelines are an extremely complex set of inclusion/exclusion criteria, supportive features, as well as red flags, whose application requires a broad and deep knowledge of neurology, and indeed of movement disorders. The MDS diagnostic recommendations can be challenging, especially for generalists with lesser expertise in neurology, movement disorders, and PD-related physical exam skills, who will be increasingly charged with the diagnosis and care of PD patients (Ou et al., 1990; Ross et al., 2022). A *meta*-analysis performed by Rizzo and colleagues (2016), reviewing 20 studies and more than 7000 patients, including 11 studies that referred to autopsy data, revealed lower PD diagnostic accuracy, with 83.9 % for movement disorder specialists who followed patients over years.101 More often, the diagnosis of PD is performed by clinicians with lesser expertise such as general neurologists, geriatricians, internists, or even family physicians, who had average diagnostic accuracies of 73.8 % for patients whom they followed over years.101 The aim is for neuroimaging measures to approach accuracy of clinical decision making of movement disorder specialists to bridge the gap, and just as repeated clinical evaluations improve diagnosis, potentially repeated scanning might increase the accuracy of classifications of these measures.

7. Limitations

One important caveat is that the generalizability of our MRI measure, and that of others in this literature, have yet to be shown, given the lack of independent samples to validate measures and models developed in training data. Furthermore, large samples of early-staged PD patients relative to HCs and PD mimics, who are tested prospectively, preferably in multicentered data, are needed. Finally, given this literature, multivariate/multimodal measures will likely be most accurate, sensitive, and specific in diagnosing PD (Martínez et al., 2023; Jokar et al., 2023), accomplished by combining QSM and neuromelanin (Martínez et al., 2023; Jokar et al., 2023; Ariz et al., 2023), as well as diffusion (Alushaj et al., 2023; Khan et al., 2019) volume (Jokar et al., 2023; Khan et al., 2019), and morphometry (Khan et al., 2019) in the SNc, N1 nigrosome, and striatum. Recent work by Nobileau and colleagues (2023) with neuromelanin MRI in the SN and the locus coeruleus suggested that combining measures across multiple subcortical subregions could distinguish between PD and PD mimics (Nobileau et al., 2023). Understanding the unique contributions of these different neuroimaging measures, at different stages and subtypes of disease, as well as the most optimal combination are required before clinical translation.

Isolation of these midbrain nuclei was achieved using the CIT168 probabilistic subcortical atlas, the first to distinguish VTA from SNc and SNr. The use of atlas-based segmentation rather than manual tracing/segmentation is a significant advantage of our approach with respect to the reproducibility of our findings (Yaakub et al., 2020). However, the CIT168 atlas used in this study has limitations. The atlas is derived using

a younger cohort. However, because both PD patients and controls are age-matched, and we have used the same atlas in both groups, this moderates the disadvantages of using an atlas derived in healthy young controls. The atlas is based only on 3T MRI data, and uses averaging of numerous brains to raise the contrast-to-noise ratio between regions for delineation (Pauli et al., 2018). Furthermore, this atlas does not restrict measures to the N1 nigrosome subregion of the SNc to allow for comparison of our measure in this subregion (Lehericy et al., 2017). The single atlas segmentation employed could be improved through multi-atlas segmentation or algorithm approaches to better define nuclei boundaries. Nonetheless, to our knowledge, no other atlases include all three midbrain nuclei thus making the CIT168 atlas the current ideal for this work.

Given the novelty of QSM, more work needs to be done to establish a gold standard method for susceptibility map generation (Yu et al., 2019). Techniques may differ in their diagnostic capacity, thus warranting comparison of various approaches for susceptibility map generation (Acosta-Cabronero et al., 2018). Furthermore, our method used a univariate threshold to define classes. More recent work highlights the advantages of incorporating whole CSF zero referencing before the inversion step rather than after, as we have implemented here (Dimov et al., 2022).

8. Conclusions

We demonstrate that QSM indexing iron in the SNc, at 3T MRI *alone*—even without incorporating clinical information or other neuroimaging measures, including neuromelanin-sensitive MRI—classified PD patients with good diagnostic accuracy in the hold-out sets of our cross-validation approach. This suggests potential of this measure to be included in multivariate and perhaps multimodal models of PD diagnosis that will have greater potential for generalizability given the challenging aim of diagnosing PD, a highly complex and heterogeneous condition. Our approach uses a publicly-available atlas to define and segment midbrain nuclei and, therefore, is entirely reproducible and can be performed by individuals with no specialized neuroradiological training. These features are strengths of the diagnostic biomarker shown here for potential clinical translation, given some pragmatic considerations, pending confirmation of these results, prospectively tested in a multicentered replication, with an entirely independent validation sample. These steps are needed for any neuroimaging measure before clinical adoption could be considered. Our findings and those studies reviewed here indicate that MRI might fulfil the promise of operating in PD as it does in most other common neurological conditions—aiding in diagnosis, staging, and prognosis. A widely-available and objective diagnostic MRI test will greatly improve clinical management of PD patients, particularly those in regions where access to neurologists and movement disorder neurologists is limited. Finally, biomarkers will improve the power of studies to investigate disease-modifying therapies and a cure for PD, where none currently exist.

Funding

This work was supported by a Canadian Institute of Health Research Project Grant ("Advancing Clinically-Useful Diagnostic and Progression Markers of PD with Neuroimaging", 201903) awarded to Dr. Penny MacDonald and Dr. Ali Khan and a BrainsCAN Accelerator Grant ("Investigating VTA, SNc and dopamine projections in the brain using MRI") arising from the Canada First Research Excellence Fund awarded to Dr. Penny MacDonald, Dr. Ali Khan, Dr. Adrian Owen, and Dr. Ravi Menon.

CRediT authorship contribution statement

Erind Alushaj: Writing – review & editing, Writing – original draft, Visualization, Investigation, Formal analysis, Data curation, Conceptualization. **Nicholas Handfield-Jones:** Data curation. **Alan Kuurstra:** Software, Methodology. **Anisa Morava:** Writing – review & editing. **Ravi S. Menon:** Methodology, Funding acquisition. **Adrian M. Owen:** Supervision, Resources, Project administration, Funding acquisition. **Manas Sharma:** Resources, Methodology. **Ali R. Khan:** Writing – review & editing, Supervision, Software, Resources, Methodology, Funding acquisition, Conceptualization. **Penny A. MacDonald:** Writing – review & editing, Writing – original draft, Supervision, Resources, Project administration, Methodology, Investigation, Funding acquisition, Conceptualization.

Declaration of competing interest

The authors declare that they have no known competing financial interests or personal relationships that could have appeared to influence the work reported in this paper.

Appendix A. Supplementary data

Supplementary data to this article can be found online at https://doi.org/10.1016/j.nicl.2024.103577.

References

Abdul-Rahman, H.S., Gdeisat, M.A., Burton, D.R., Lalor, M.J., Lilley, F., Moore, C.J., 2007. Fast and robust three-dimensional best path phase unwrapping algorithm. Appl. Opt. 46 (26), 6623–6635. https://doi.org/10.1364/AO.46.006623.

Acosta-Cabronero, J., Cardenas-Blanco, A., Betts, M.J., et al., 2017. The whole-brain pattern of magnetic susceptibility perturbations in Parkinson's disease. Brain 140 (1), 118–131. https://doi.org/10.1093/brain/aww278.

Acosta-Cabronero, J., Milovic, C., Mattern, H., Tejos, C., Speck, O., Callaghan, M.F., 2018. A robust multi-scale approach to quantitative susceptibility mapping. Neuroimage 183, 7–24. https://doi.org/10.1016/j.neuroimage.2018.07.065.

Ahmadi, S.A., Bötzel, K., Levin, J., et al., 2020. Analyzing the co-localization of substantia nigra hyper-echogenicities and iron accumulation in Parkinson's disease: a multi-modal atlas study with transcranial ultrasound and MRI. Neuroimage Clin. 26, 102185 https://doi.org/10.1016/j.nicl.2020.102185.

Alberico, S.L., Cassell, M.D., Narayanan, N.S., 2015. The Vulnerable Ventral Tegmental Area in Parkinson's Disease. Basal Ganglia 5 (2–3), 51–55. https://doi.org/10.1016/j.baga.2015.06.001.

Ali, K., Morris, H.R., 2015. Parkinson's disease: chameleons and mimics. Pract. Neurol. 15 (1), 14–25. https://doi.org/10.1136/practneurol-2014-000849.

Alushaj, E., Hemachandra, D., Kuurstra, A., et al., 2023. Subregional analysis of striatum iron in Parkinson's disease and rapid eye movement sleep behaviour disorder. Neuroimage Clin. 40. https://doi.org/10.1016/j.nicl.2023.103519.

An, H., Zeng, X., Niu, T., et al., 2018. Quantifying iron deposition within the substantia nigra of Parkinson's disease by quantitative susceptibility mapping. J. Neurol. Sci. 386, 46–52. https://doi.org/10.1016/j.jns.2018.01.008.

Archer, D.B., Bricker, J.T., Chu, W.T., et al., 2019. Development and validation of the automated imaging differentiation in Parkinsonism (AID-P): a multicentre machine learning study. Lancet Digit Health 1 (5), e222–e231. https://doi.org/10.1016/S2589-7500(19)30105-0.

Ariz, M., Martínez, M., Alvarez, I., et al. Automatic segmentation and quantification of nigrosome-1 neuromelanin and iron in MRI: a candidate biomarker for Parkinson's disease The Catalonian Neuroimaging Parkinson's disease. Consortium. doi: 10.1101/2023.04.13.23288519.

Avants, B., Tustison, N., Song, G., 2008. Advanced normalization tools (ANTS). Insight J. 1–35. https://doi.org/10.54294/uvnhin.

Ayton, S., Lei, P., 2014. Nigral iron elevation is an invariable feature of Parkinson's disease and is a sufficient cause of neurodegeneration. Biomed. Res. Int. 2014, 581256 https://doi.org/10.1155/2014/581256.

Azuma, M., Hirai, T., Yamada, K., et al., 2016. Lateral asymmetry and spatial difference of iron deposition in the substantia nigra of patients with Parkinson disease measured with quantitative susceptibility mapping. AJNR Am. J. Neuroradiol. 37 (5), 782–788. https://doi.org/10.3174/ajnr.A4645.

Azuma, M., Hirai, T., Nakaura, T., et al., 2019. Combining quantitative susceptibility mapping to the morphometric index in differentiating between progressive supranuclear palsy and Parkinson's disease. J. Neurol. Sci. 406, 116443 https://doi.org/10.1016/j.jns.2019.116443.

Bae, Y.J., Kim, J., Kim, E., et al., 2016. Loss of nigral hyperintensity on 3 Tesla MRI of Parkinsonism: comparison with 123I-FP-CIT SPECT. Mov. Disord. 31 (5), 684–692.

Barbosa, J.H., Santos, A.C., Tumas, V., et al., 2015. Quantifying brain iron deposition in patients with Parkinson's disease using quantitative susceptibility mapping, R2 and R2. Magn. Reson Imaging 33 (5), 559–565. https://doi.org/10.1016/j.mri.2015.02.021.

Barone, P., Antonini, A., Colosimo, C., et al., 2009. The PRIAMO study: a multicenter assessment of nonmotor symptoms and their impact on quality of life in Parkinson's disease. Mov. Disord. 24 (11), 1641–1649. https://doi.org/10.1002/mds.22643.

Benjamini, Y., Hochberg, Y., 1995. Controlling the false discovery rate: a practical and powerful approach to multiple testing. J. R. Stat. Soc.: Ser. B (Methodological) 57 (1), 289–300. https://doi.org/10.1111/j.2517-6161.1995.tb02031.x.
Bergsland, N., Schweser, F., Dwyer, M.G., Weinstock-Guttman, B., Benedict, R.H.B., Zivadinov, R., 2018. Thalamic white matter in multiple sclerosis: a combined diffusion-tensor imaging and quantitative susceptibility mapping study. Hum. Brain Mapp. 39 (10), 4007–4017. https://doi.org/10.1002/hbm.24227.
Biondetti, E., Gaurav, R., Yahia-Cherif, L., et al., 2020. Spatiotemporal changes in substantia nigra neuromelanin content in Parkinson's disease. Brain 143 (9), 2757–2770.
Biondetti, E., Santin, M.D., Valabrègue, R., et al., 2021. The spatiotemporal changes in dopamine, neuromelanin and iron characterizing Parkinson's disease. Brain 144 (10), 3114–3125. https://doi.org/10.1093/brain/awab191.
Cassidy, C.M., Zucca, F.A., Girgis, R.R., et al., 2019. Neuromelanin-sensitive MRI as a noninvasive proxy measure of dopamine function in the human brain. Proc. Natl. Acad. Sci. U.S.A. 116 (11), 5108–5117. https://doi.org/10.1073/pnas.1807983116.
Chatnuntawech, I., McDaniel, P., Cauley, S.F., et al., 2017. Single-step quantitative susceptibility mapping with variational penalties. NMR Biomed. 30 (4) https://doi.org/10.1002/nbm.3570.
Chau, M.T., Todd, G., Wilcox, R., Agzarian, M., Bezak, E., 2020. Diagnostic accuracy of the appearance of Nigrosome-1 on magnetic resonance imaging in Parkinson's disease: a systematic review and meta-analysis. Parkinsonism Relat. Disord. 78, 12–20. https://doi.org/10.1016/j.parkreldis.2020.07.002.
Chen, Q., Chen, Y., Zhang, Y., et al., 2019. Iron deposition in Parkinson's disease by quantitative susceptibility mapping. BMC Neurosci. 20 (1), 23. https://doi.org/10.1186/s12868-019-0505-9.
Cheng, Z., Zhang, J., He, N., et al., 2019. Radiomic features of the nigrosome-1 region of the Substantia Nigra: using quantitative susceptibility mapping to assist the diagnosis of idiopathic Parkinson's disease. Front. Aging Neurosci. 11, 167. https://doi.org/10.3389/fnagi.2019.00167.
Chougar, L., Faouzi, J., Pyatigorskaya, N., et al., 2021. Automated categorization of parkinsonian syndromes using magnetic resonance imaging in a clinical setting. Mov. Disord. 36 (2), 460–470.
Chougar, L., Arsovic, E., Gaurav, R., et al., 2022. Regional selectivity of neuromelanin changes in the substantia Nigra in atypical Parkinsonism. Mov. Disord. 37 (6), 1245–1255. https://doi.org/10.1002/mds.28988.
De, M.R., Poewe, W., Gizewski, E.R., Mahlknecht, P., Seppi, K., 2016. Utility of nigral signal intensity changes on MR images to differentiate drug-induced Parkinsonism from Parkinson disease. Radiology 281 (2), 651–652.
De Rochefort, L., Liu, T., Kressler, B., et al., 2010. Quantitative susceptibility map reconstruction from MR phase data using bayesian regularization: validation and application to brain imaging. Magn. Reson Med. 63 (1), 194–206. https://doi.org/10.1002/mrm.22187.
Deistung, A., Rauscher, A., Sedlacik, J., Stadler, J., Witoszynskyj, S., Reichenbach, J.R., 2008. Susceptibility weighted imaging at ultra high magnetic field strengths: theoretical considerations and experimental results. Magn. Reson Med. 60 (5), 1155–1168. https://doi.org/10.1002/mrm.21754.
Deistung, A., Schafer, A., Schweser, F., Biedermann, U., Turner, R., Reichenbach, J.R., 2013. Toward in vivo histology: a comparison of quantitative susceptibility mapping (QSM) with magnitude-, phase-, and R2*-imaging at ultra-high magnetic field strength. Neuroimage 65, 299–314. https://doi.org/10.1016/j.neuroimage.2012.09.055.
Deistung, A., Schweser, F., Reichenbach, J.R., 2017. Overview of quantitative susceptibility mapping. NMR Biomed. 30 (4) https://doi.org/10.1002/nbm.3569.
Dexter, D.T., Carayon, A., Javoy-Agid, F., et al., 1991. Alterations in the levels of iron, ferritin and other trace metals in Parkinson's disease and other neurodegenerative diseases affecting the basal ganglia. Brain 114.
Dimov, A.V., Nguyen, T.D., Spincemaille, P., et al., 2022. Global cerebrospinal fluid as a zero-reference regularization for brain quantitative susceptibility mapping. J. Neuroimaging 32 (1), 141–147. https://doi.org/10.1111/jon.12923.
Du, G., Lewis, M.M., Styner, M., et al., 2011. Combined R2* and diffusion tensor imaging changes in the substantia nigra in Parkinson's disease. Mov. Disord. 26 (9), 1627–1632. https://doi.org/10.1002/mds.23643.
Du, G., Liu, T., Lewis, M.M., et al., 2016. Quantitative susceptibility mapping of the midbrain in Parkinson's disease. Mov. Disord. 31 (3), 317–324. https://doi.org/10.1002/mds.26417.
Du, L., Zhao, Z., Cui, A., et al., 2018. Increased iron deposition on brain quantitative susceptibility mapping correlates with decreased cognitive function in Alzheimer's disease. ACS Chem. Neurosci. 9 (7), 1849–1857. https://doi.org/10.1021/acschemneuro.8b00194.
Eapen, M., Zald, D.H., Gatenby, J.C., Ding, Z., Gore, J.C., 2011. Using high-resolution MR imaging at 7T to evaluate the anatomy of the midbrain dopaminergic system. AJNR Am. J. Neuroradiol. 32 (4), 688–694. https://doi.org/10.3174/ajnr.A2355.
Eskildsen, S.F., Coupé, P., Fonov, V., et al., 2012. BEaST: brain extraction based on nonlocal segmentation technique. Neuroimage 59 (3), 2362–2373. https://doi.org/10.1016/j.neuroimage.2011.09.012.
Ghassaban, K., Liu, S., Jiang, C., Haacke, E.M., 2019. Quantifying iron content in magnetic resonance imaging. Neuroimage 187, 77–92. https://doi.org/10.1016/j.neuroimage.2018.04.047.
Goetz, C.G., Poewe, W., Rascol, O., et al., 2004. Movement Disorder Society Task Force report on the Hoehn and Yahr staging scale: status and recommendations. Mov. Disord. 19 (9), 1020–1028. https://doi.org/10.1002/mds.20213.
Goetz, C.G., Tilley, B.C., Shaftman, S.R., et al., 2008. Movement Disorder Society-Sponsored Revision of the Unified Parkinson's Disease Rating Scale (MDS-UPDRS): scale presentation and clinimetric testing results. Mov. Disord. 23 (15), 2129–2170. https://doi.org/10.1002/mds.22340.
Guan, X., Xuan, M., Gu, Q., et al., 2017. Influence of regional iron on the motor impairments of Parkinson's disease: a quantitative susceptibility mapping study. J. Magn. Reson. Imaging 45 (5), 1335–1342. https://doi.org/10.1002/jmri.25434.
Guan, X., Xuan, M., Gu, Q., et al., 2017. Regionally progressive accumulation of iron in Parkinson's disease as measured by quantitative susceptibility mapping. NMR Biomed. 30 (4) https://doi.org/10.1002/nbm.3489.
Guan, X., Zhang, Y., Wei, H., et al., 2019. Iron-related nigral degeneration influences functional topology mediated by striatal dysfunction in Parkinson's disease. Neurobiol. Aging 75, 83–97. https://doi.org/10.1016/j.neurobiolaging.2018.11.013.
Hanley, J.A., McNeil, B.J., 1983. A method of comparing the areas under receiver operating characteristic curves derived from the same cases. Radiology 148 (3), 839–843. https://doi.org/10.1148/radiology.148.3.6878708.
Hardman, C.D., McRitchie, D.A., Halliday, G.M., Cartwright, H.R., Morris, J.G., 1996. Substantia nigra pars reticulata neurons in Parkinson's disease. Neurodegeneration 5 (1), 49–55.
Hare, D.J., Lei, P., Ayton, S., et al., 2014. An iron–dopamine index predicts risk of parkinsonian neurodegeneration in the substantia nigra pars compacta. Chem. Sci. 5 (6), 2160–2169. https://doi.org/10.1039/c3sc53461h.
He, N., Ling, H., Ding, B., et al., 2015. Region-specific disturbed iron distribution in early idiopathic Parkinson's disease measured by quantitative susceptibility mapping. Hum. Brain Mapp. 36 (11), 4407–4420. https://doi.org/10.1002/hbm.22928.
He, N., Ghassaban, K., Huang, P., et al., 2021. Imaging iron and neuromelanin simultaneously using a single 3D gradient echo magnetization transfer sequence: combining neuromelanin, iron and the nigrosome-1 sign as complementary imaging biomarkers in early stage Parkinson's disease. Neuroimage 230, 117810. https://doi.org/10.1016/j.neuroimage.2021.117810.
He, N., Chen, Y., LeWitt, P.A., Yan, F., Haacke, E.M., 2023. Application of neuromelanin MR imaging in Parkinson disease. J. Magn. Reson. Imaging 57 (2), 337–352. https://doi.org/10.1002/jmri.28414.
Hoehn, M.M., Yahr, M.D., 1967. Parkinsonism. Neurology 17 (5), 427. https://doi.org/10.1212/WNL.17.5.427.
Huddleston, D.E., Langley, J., Sedlacik, J., Boelmans, K., Factor, S.A., Hu, X.P., 2017. In vivo detection of lateral-ventral tier nigral degeneration in Parkinson's disease. Hum. Brain Mapp. 38 (5), 2627–2634. https://doi.org/10.1002/hbm.23547.
Hughes, A.J., Daniel, S.E., Kilford, L., Lees, A.J., 1992. Accuracy of clinical diagnosis of idiopathic Parkinson's disease: a clinico-pathological study of 100 cases. J. Neurol. Neurosurg. Psychiatry 55 (3), 181–184. https://doi.org/10.1136/jnnp.55.3.181.
Jenkinson, M., Beckmann, C.F., Behrens, T.E., Woolrich, M.W., Smith, S.M., 2012. FSL. Neuroimage 62 (2), 782–790. https://doi.org/10.1016/j.neuroimage.2011.09.015.
Jokar, M., Jin, Z., Huang, P., et al., 2023. Diagnosing Parkinson's disease by combining neuromelanin and iron imaging features using an automated midbrain template approach. Neuroimage 266. https://doi.org/10.1016/j.neuroimage.2022.119814.
Khan, A.R., Hiebert, N.M., Vo, A., et al., 2019. Biomarkers of Parkinson's disease: striatal sub-regional structural morphometry and diffusion MRI. Neuroimage Clin. 21, 101597 https://doi.org/10.1016/j.nicl.2018.11.007.
Kim, E.Y., Sung, Y.H., Lee, J., 2019. Nigrosome 1 Imaging: Technical Considerations and Clinical Applications. vol 92.
Kim, E.Y., Sung, Y.H., Shin, H.G., Noh, Y., Nam, Y., Lee, J., 2018. Diagnosis of early-stage idiopathic parkinson's disease using high-resolution quantitative susceptibility mapping combined with histogram analysis in the substantia Nigra at 3 T. J. Clin. Neurol. 14 (1), 90–97. https://doi.org/10.3988/jcn.2018.14.1.90.
Kish, S.J., Shannak, K., Hornykiewicz, O., 1988. Uneven pattern of dopamine loss in the striatum of patients with idiopathic Parkinson's disease. Pathophysiologic and clinical implications. N. Engl. J. Med. 318 (14), 876–880. https://doi.org/10.1056/NEJM198804073181402.
Klassen, L.M., Menon, R.S., 2013. Optimal phase sensitive combination of multi-channel, multi-echo images. In: Proceedings of the 21st Annual Meeting of ISMRM, Salt Lake City, Utah.
Kubis, N., Faucheux, B.A., Ransmayr, G., et al., 2000. Preservation of midbrain catecholaminergic neurons in very old human subjects. Brain 123 (2), 366–373. https://doi.org/10.1093/brain/123.2.366.
Lancione, M., Donatelli, G., Del Prete, E., et al., 2022. Evaluation of iron overload in nigrosome 1 via quantitative susceptibility mapping as a progression biomarker in prodromal stages of synucleinopathies. Neuroimage 260. https://doi.org/10.1016/j.neuroimage.2022.119454.
Langkammer, C., Schweser, F., Krebs, N., et al., 2012. Quantitative susceptibility mapping (QSM) as a means to measure brain iron? A post mortem validation study. Neuroimage 62 (3), 1593–1599. https://doi.org/10.1016/j.neuroimage.2012.05.049.
Langkammer, C., Pirpamer, L., Seiler, S., et al., 2016. Quantitative susceptibility mapping in Parkinson's disease. PLoS One 11 (9), e0162460.
Lautenschläger, J., Stephens, A.D., Fusco, G., et al., 2018. C-terminal calcium binding of α-synuclein modulates synaptic vesicle interaction. Nat. Commun. 9 (1) https://doi.org/10.1038/s41467-018-03111-4.
Lee, H., Cho, H., Lee, M.J., Kim, T.H., Roh, J., Lee, J.H., 2021. Differential effect of iron and myelin on susceptibility MRI in the Substantia Nigra. Radiology 301 (3), 682–691. https://doi.org/10.1148/radiol.2021210116.
Lee, D.Y., Chung, C.K., Hwang, Y.S., et al., 2000. Dysembryoplastic neuroepithelial tumor: radiological findings (including PET, SPECT, and MRS) and surgical strategy. J. Neurooncol. 47 (2), 167–174.
Lehericy, S., Vaillancourt, D.E., Seppi, K., et al., 2017. The role of high-field magnetic resonance imaging in parkinsonian disorders: Pushing the boundaries forward. Mov. Disord. 32 (4), 510–525. https://doi.org/10.1002/mds.26968.
Levenberg, K., 1944. A method for the solution of certain non – linear problems in least squares. Q. Appl. Math. 2, 164–168.

Li, K.R., Avecillas-Chasin, J., Nguyen, T.D., et al., 2022. Quantitative evaluation of brain iron accumulation in different stages of Parkinson's disease. J. Neuroimaging 32 (2), 363–371. https://doi.org/10.1111/jon.12957.
Li, X., Chen, L., Kutten, K., et al., 2019. Multi-atlas tool for automated segmentation of brain gray matter nuclei and quantification of their magnetic susceptibility. Neuroimage 191, 337–349. https://doi.org/10.1016/j.neuroimage.2019.02.016.
Liu, Q., Wang, P., Liu, C., et al., 2023. An investigation of neuromelanin distribution in substantia nigra and locus coeruleus in patients with Parkinson's disease using neuromelanin-sensitive MRI. BMC Neurol. 23 (1) https://doi.org/10.1186/s12883-023-03350-z.
Lotfipour, A.K., Wharton, S., Schwarz, S.T., et al., 2012. High resolution magnetic susceptibility mapping of the substantia nigra in Parkinson's disease. J. Magn. Reson. Imaging 35 (1), 48–55. https://doi.org/10.1002/jmri.22752.
Mahlknecht, P., Krismer, F., Poewe, W., Seppi, K., 2017. Meta-analysis of dorsolateral nigral hyperintensity on magnetic resonance imaging as a marker for Parkinson's disease. Mov. Disord. 32 (4), 619–623. https://doi.org/10.1002/mds.26932.
Mak, E., Su, L., Williams, G.B., O'Brien, J.T., 2015. Neuroimaging correlates of cognitive impairment and dementia in Parkinson's disease. Parkinsonism Relat. Disord. 21 (8), 862–870. https://doi.org/10.1016/j.parkreldis.2015.05.013.
Marquardt, D.W., 1963. An algorithm for least-squares estimation of nonlinear parameters. J. Soc. Ind. Appl. Math. 11 (2), 431–441. https://doi.org/10.1137/0111030.
Martínez, M., Ariz, M., Alvarez, I., et al., 2023. Brainstem neuromelanin and iron MRI reveals a precise signature for idiopathic and LRRK2 Parkinson's disease. NPJ Parkinsons Dis. 9 (1) https://doi.org/10.1038/s41531-023-00503-2.
Martinez-Martin, P., Urra, D.G., del Ser, Q.T., et al., 1997. A new clinical tool for gait evaluation in Parkinson's disease. Clin. Neuropharmacol. 20 (3), 183–194.
McCleery, J., Morgan, S., Bradley, K.M., Noel-Storr, A.H., Ansorge, O., Hyde, C., 2015. Dopamine transporter imaging for the diagnosis of dementia with Lewy bodies. Cochrane Database Syst. Rev. 2017 (6) https://doi.org/10.1002/14651858.CD010633.pub2.
McRitchie, D.A., Hardman, C.D., Halliday, G.M., 1996. Cytoarchitectural distribution of calcium binding proteins in midbrain dopaminergic regions of rats and humans. J. Comp. Neurol. 364 (1), 121–150. https://doi.org/10.1002/(SICI)1096-9861(19960101)364:1<121::AID-CNE11>3.0.CO;2-1.
Meijer, F.J.A., van Rumund, A., Fasen, B.A.C.M., et al., 2015. Susceptibility-weighted imaging improves the diagnostic accuracy of 3T brain MRI in the work-up of Parkinsonism. Am. J. Neuroradiol. 36 (3), 454–460.
Miller, D.B., O'Callaghan, J.P., 2015. Biomarkers of Parkinson's disease: present and future. Metabolism 64 (3 Suppl 1), S40–S46. https://doi.org/10.1016/j.metabol.2014.10.030.
Mitchell, T., Lehéricy, S., Chiu, S.Y., Strafella, A.P., Stoessl, A.J., Vaillancourt, D.E., 2021. Emerging neuroimaging biomarkers across disease stage in Parkinson disease: a review. JAMA Neurol. 78 (10), 1262–1272. https://doi.org/10.1001/jamaneurol.2021.1312.
Modat, M., Ridgway, G.R., Taylor, Z.A., et al., 2010. Fast free-form deformation using graphics processing units. Comput. Methods Programs Biomed. 98 (3), 278–284. https://doi.org/10.1016/j.cmpb.2009.09.002.
Modat, M., Cash, D.M., Daga, P., Winston, G.P., Duncan, J.S., Ourselin, S., 2014. Global image registration using a symmetric block-matching approach. J. Med. Imaging (Bellingham) 1 (2), 24003. https://doi.org/10.1117/1.JMI.1.2.024003.
Moos, T., Morgan, E.H., 2004. The metabolism of neuronal iron and its pathogenic role in neurological disease: review. Ann. N. Y. Acad. Sci. 1012 (1), 14–26. https://doi.org/10.1196/annals.1306.002.
Murakami, Y., Kakeda, S., Watanabe, K., et al., 2015. Usefulness of quantitative susceptibility mapping for the diagnosis of Parkinson disease. AJNR Am. J. Neuroradiol. 36 (6), 1102–1108. https://doi.org/10.3174/ajnr.A4260.
Nasreddine, Z.S., Phillips, N.A., Bedirian, V., et al., 2005. The Montreal Cognitive Assessment, MoCA: a brief screening tool for mild cognitive impairment. J. Am. Geriatr. Soc. 53 (4), 695–699. https://doi.org/10.1111/j.1532-5415.2005.53221.x.
Nobileau, A., Gaurav, R., Chougar, L., et al., 2023. Neuromelanin-sensitive magnetic resonance imaging changes in the locus coeruleus/subcoeruleus complex in patients with typical and atypical Parkinsonism. Mov. Disord. 38 (3), 479–484. https://doi.org/10.1002/mds.29309.
Noh, Y., Sung, Y.H., Lee, J., Kim, E.Y., 2015. Nigrosome 1 detection at 3T MRI for the diagnosis of early-stage idiopathic Parkinson disease: assessment of diagnostic accuracy and agreement on imaging asymmetry and clinical laterality. Am. J. Neuroradiol. 36 (11), 2010–2016.
Ofori, E., Pasternak, O., Planetta, P.J., et al., 2015. Longitudinal changes in free-water within the substantia nigra of Parkinson's disease. Brain 138 (8), 2322–2331. https://doi.org/10.1093/brain/awv136.
Ohtsuka, C., Sasaki, M., Konno, K., et al., 2014. Differentiation of early-stage parkinsonisms using neuromelanin-sensitive magnetic resonance imaging. Parkinsonism Relat. Disord. 20 (7), 755–760.
Okunoye, O., Marston, L., Walters, K., Schrag, A., 2022. Change in the incidence of Parkinson's disease in a large UK primary care database. NPJ Parkinsons Dis. 8 (1) https://doi.org/10.1038/s41531-022-00284-0.
Ou, Z., Pan, J., Tang, S., et al., 2021. Global trends in the incidence, prevalence, and years lived with disability of Parkinson's disease in 204 countries/territories from 1990 to 2019. Front. Public Health 9. https://doi.org/10.3389/fpubh.2021.776847.
Pauli, J.L., Chen, J.Y., Basiri, M.L., et al., 2022. Molecular and anatomical characterization of parabrachial neurons and their axonal projections. Elife 11. https://doi.org/10.7554/eLife.81868.
Pauli, W.M., Nili, A.N., Tyszka, J.M., 2018. A high-resolution probabilistic in vivo atlas of human subcortical brain nuclei. Sci. Data 5, 180063. https://doi.org/10.1038/sdata.2018.63.
Pautrat, A., Al Tannir, R., Pernet-Gallay, K., et al., 2023. Altered parabrachial nucleus nociceptive processing may underlie central pain in Parkinson's disease. NPJ Parkinsons Dis. 9 (1) https://doi.org/10.1038/s41531-023-00516-x.
Peckham, M.E., Dashtipour, K., Holshouser, B.A., et al., 2016. Novel pattern of iron deposition in the fascicula nigrale in patients with Parkinson's disease: a pilot study. Radiol Res Pract. 2016, 9305018. https://doi.org/10.1155/2016/9305018.
Peralta, C., Strafella, A.P., van Eimeren, T., et al., 2022. Pragmatic approach on neuroimaging techniques for the differential diagnosis of Parkinsonisms. Mov. Disord. Clin. Pract. 9 (1), 6–19. https://doi.org/10.1002/mdc3.13354.
Perez Akly, M.S., Stefani, C.V., Ciancaglini, L., et al., 2019. Accuracy of nigrosome-1 detection to discriminate patients with Parkinson's disease and essential tremor. Neuroradiol. J. 32 (6), 395–400. https://doi.org/10.1177/1971400919853787.
Persson, N., Wu, J., Zhang, Q., et al., 2015. Age and sex related differences in subcortical brain iron concentrations among healthy adults. Neuroimage 122, 385–398. https://doi.org/10.1016/j.neuroimage.2015.07.050.
Plouvier, A.O.A., Hartman, T.C.O., Verhulst, C.E.M., Bloem, B.R., van Weel, C., Lagro-Janssen, A.L.M., 2017. Parkinson's disease: patient and general practitioner perspectives on the role of primary care. Fam. Pract. 34 (2), 227–233. https://doi.org/10.1093/fampra/cmw115.
Postuma, R.B., Berg, D., Stern, M., et al., 2015. MDS clinical diagnostic criteria for Parkinson's disease. Mov. Disord. 30 (12), 1591–1601. https://doi.org/10.1002/mds.26424.
Prasad, S., Stezin, A., Lenka, A., et al., 2018. Three-dimensional neuromelanin-sensitive magnetic resonance imaging of the substantia nigra in Parkinson's disease. Eur. J. Neurol. 25 (4), 680–686. https://doi.org/10.1111/ene.13573.
Prasuhn, J., Neumann, A., Strautz, R., et al., 2021. Clinical MR imaging in Parkinson's disease: how useful is the swallow tail sign? Brain Behav. 11 (7) https://doi.org/10.1002/brb3.2202.
Pyatigorskaya, N., Magnin, B., Mongin, M., et al., 2018. Comparative study of MRI biomarkers in the Substantia Nigra to discriminate idiopathic Parkinson disease. AJNR Am. J. Neuroradiol. 39 (8), 1460–1467. https://doi.org/10.3174/ajnr.A5702.
Pyatigorskaya, N., Sanz-Morère, C.B., Gaurav, R., et al., 2020. Iron imaging as a diagnostic tool for Parkinson's disease: a systematic review and meta-analysis. Front. Neurol. 11 (366) https://doi.org/10.3389/fneur.2020.00366.
Ratliff, J.B., Schaefer, S.M., Chitnis, S., et al., 2022. Viewpoint on milestones for fellowship training in movement disorders. Mov. Disord. 37 (8), 1605–1609. https://doi.org/10.1002/mds.29146.
Ravanfar, P., Loi, S.M., Syeda, W.T., et al., 2021. Systematic review: quantitative susceptibility mapping (QSM) of brain iron profile in neurodegenerative diseases. Front. Neurosci. 15 (February) https://doi.org/10.3389/fnins.2021.618435.
Rizzo, G., Copetti, M., Arcuti, S., Martino, D., Fontana, A., Logroscino, G., 2016. Accuracy of clinical diagnosis of Parkinson disease. Neurology 86 (6), 566–576. https://doi.org/10.1212/WNL.0000000000002350.
Rolheiser, T.M., Fulton, H.G., Good, K.P., et al., 2011. Diffusion tensor imaging and olfactory identification testing in early-stage Parkinson's disease. J. Neurol. 258 (7), 1254–1260.
Ross, S.C., Jakkampudi, V., Jens, W., Barbush, K., Sathian, K., Huang, X., 2022. Improving access to tertiary movement disorders subspecialty care: a team model born from the COVID-19 crisis. Neurol. Clin. Pract. 12 (2), 164–168. https://doi.org/10.1212/CPJ.0000000000001154.
Schindlbeck, K.A., Vo, A., Mattis, P.J., et al., 2021. Cognition-related functional topographies in Parkinson's disease: localized loss of the ventral default mode network. Cereb. Cortex 31 (11), 5139–5150.
Sederman, A.J., 2022. Magnetic resonance imaging. In: Industrial Tomography: Systems and Applications, second ed. Elsevier. pp. 127–153. doi:10.1016/B978-0-12-823015-2.00003-0.
Sethi, S.K., Kisch, S.J., Ghassaban, K., et al., 2019. Iron quantification in Parkinson's disease using an age-based threshold on susceptibility maps: the advantage of local versus entire structure iron content measurements. Magn. Reson. Imaging 55, 145–152. https://doi.org/10.1016/j.mri.2018.10.001.
Shahmaei, V., Faeghi, F., Mohammdbeigi, A., Hashemi, H., Ashrafi, F., 2019. Evaluation of iron deposition in brain basal ganglia of patients with Parkinson's disease using quantitative susceptibility mapping. Eur. J. Radiol. Open 6, 169–174. https://doi.org/10.1016/j.ejro.2019.04.005.
Shams, S., Fällmar, D., Schwarz, S., et al., 2017. MRI of the swallow tail sign: a useful marker in the diagnosis of lewy body dementia? Am. J. Neuroradiol. 38 (9), 1737–1741. https://doi.org/10.3174/ajnr.A5274.
Shimada, H., Hirano, S., Shinotoh, H., et al., 2009. Mapping of brain acetylcholinesterase alterations in Lewy body disease by PET. Neurology 73 (4), 273–278.
Sjöström, H., Granberg, T., Westman, E., Svenningsson, P., 2017. Quantitative susceptibility mapping differentiates between parkinsonian disorders. Parkinsonism Relat. Disord. 44, 51–57. https://doi.org/10.1016/j.parkreldis.2017.08.029.
Song, T., Li, J., Mei, S., et al., 2021. Nigral iron deposition is associated with levodopa-induced dyskinesia in Parkinson's disease. Front. Neurosci. 15, 214.
Sun, J., Lai, Z., Ma, J., et al., 2020. Quantitative evaluation of iron content in idiopathic rapid eye movement sleep behavior disorder. Mov. Disord. 35 (3), 478–485. https://doi.org/10.1002/mds.27929.
Takahashi, H., Watanabe, Y., Tanaka, H., et al., 2018. Quantifying changes in nigrosomes using quantitative susceptibility mapping and neuromelanin imaging for the diagnosis of early-stage Parkinson's disease. Br. J. Radiol. 91 (1086), 20180037. https://doi.org/10.1259/bjr.20180037.
Takahashi, H., Watanabe, Y., Tanaka, H., et al., 2018. Comprehensive MRI quantification of the substantia nigra pars compacta in Parkinson's disease. Eur. J. Radiol. 109, 48–56. https://doi.org/10.1016/j.ejrad.2018.06.024.

Tan, S., Hartono, S., Welton, T., et al., 2021. Utility of quantitative susceptibility mapping and diffusion kurtosis imaging in the diagnosis of early Parkinson's disease. Neuroimage Clin. 32, 102831 https://doi.org/10.1016/j.nicl.2021.102831.

Tang, C.C., Poston, K.L., Eckert, T., et al., 2010. Differential diagnosis of parkinsonism: a metabolic imaging study using pattern analysis. Lancet Neurol. 9 (2), 149–158. https://doi.org/10.1016/S1474-4422(10)70002-8.

Thomas, G.E.C., Leyland, L.A., Schrag, A.E., Lees, A.J., Acosta-Cabronero, J., Weil, R.S., 2020. Brain iron deposition is linked with cognitive severity in Parkinson's disease. J. Neurol. Neurosurg. Psychiatry 91 (4), 418–425. https://doi.org/10.1136/jnnp-2019-322042.

Trutti, A.C., Mulder, M.J., Hommel, B., Forstmann, B.U., 2019. Functional neuroanatomical review of the ventral tegmental area. Neuroimage 191, 258–268. https://doi.org/10.1016/j.neuroimage.2019.01.062.

Uchida, Y., Kan, H., Sakurai, K., et al., 2019. Voxel-based quantitative susceptibility mapping in Parkinson's disease with mild cognitive impairment. Mov. Disord. Published Online. https://doi.org/10.1002/mds.27717.

Uchida, Y., Kan, H., Sakurai, K., et al., 2019. Voxel-based quantitative susceptibility mapping in Parkinson's disease with mild cognitive impairment. Mov. Disord. 34 (8), 1164–1173. https://doi.org/10.1002/mds.27717.

Uchida, Y., Kan, H., Sakurai, K., et al., 2020. Magnetic susceptibility associates with dopaminergic deficits and cognition in Parkinson's disease. Mov. Disord. 35 (8), 1396–1405. https://doi.org/10.1002/mds.28077.

Vaillancourt, D.E., Spraker, M.B., Prodoehl, J., et al., 2009. High-resolution diffusion tensor imaging in the substantia nigra of de novo Parkinson disease. Neurology 72 (16), 1378–1384. https://doi.org/10.1212/01.wnl.0000340982.01727.6e.

Virameteekul, S., Revesz, T., Jaunmuktane, Z., Warner, T.T., De Pablo-Fernández, E., 2023. Clinical diagnostic accuracy of Parkinson's disease: where do we stand? Mov. Disord. Published Online. https://doi.org/10.1002/mds.29317.

Walsh, D.O., Gmitro, A.F., Marcellin, M.W., 2000. Adaptive reconstruction of phased array MR imagery. Magn. Reson. Med. 43 (5), 682–690.

Wang, E.W., Brown, G.L., Lewis, M.M., et al., 2023. Susceptibility magnetic resonance imaging correlates with glial density and Tau in the Substantia Nigra Pars compacta. Mov. Disord. 38 (3), 464–473. https://doi.org/10.1002/mds.29311.

Wang, S., Wu, T., Cai, Y., Yu, Y., Chen, X., Wang, L., 2023. Neuromelanin magnetic resonance imaging of substantia nigra and locus coeruleus in Parkinson's disease with freezing of gait. Front. Aging Neurosci. 15. https://doi.org/10.3389/fnagi.2023.1060935.

Wang, N., Yang, H.G., Li, C.B., Fan, G.G., Luo, X.G., 2017. Using 'swallow-tail' sign and putaminal hypointensity as biomarkers to distinguish multiple system atrophy from idiopathic Parkinson's disease: a susceptibility-weighted imaging study. Eur. Radiol. 27 (8), 3174–3180. https://doi.org/10.1007/s00330-017-4743-x.

Wang, J.Y., Zhuang, Q.Q., Zhu, L.B., et al., 2016. Meta-analysis of brain iron levels of Parkinson's disease patients determined by postmortem and MRI measurements. Sci. Rep. 6, 36669. https://doi.org/10.1038/srep36669.

Wüllner, U., Kassubek, J., Odin, P., et al., 2010. Transdermal rotigotine for the perioperative management of Parkinson's disease. J. Neural Transm. (Vienna) 117 (7), 855–859. https://doi.org/10.1007/s00702-010-0425-4.

Xiao, B., He, N., Wang, Q., et al., 2021. Stability of AI-enabled diagnosis of Parkinson's disease: a study targeting substantia nigra in quantitative susceptibility mapping imaging. Front. Neurosci. 15.

Xuan, M., Guan, X., Gu, Q., et al., 2017. Different iron deposition patterns in early- and middle-late-onset Parkinson's disease. Parkinsonism Relat. Disord. 44, 23–27. https://doi.org/10.1016/j.parkreldis.2017.08.013.

Yaakub, S.N., Heckemann, R.A., Keller, S.S., McGinnity, C.J., Weber, B., Hammers, A., 2020. On brain atlas choice and automatic segmentation methods: a comparison of MAPER & FreeSurfer using three atlas databases. Sci. Rep. 10 (1), 1–15. https://doi.org/10.1038/s41598-020-57951-6.

Yu, F.F., Chiang, F.L., Stephens, N., et al., 2019. Characterization of normal-appearing white matter in multiple sclerosis using quantitative susceptibility mapping in conjunction with diffusion tensor imaging. Neuroradiology 61 (1), 71–79. https://doi.org/10.1007/s00234-018-2137-7.

Zhang, D., Yao, J., Sun, J., et al., 2023. Iron accumulation in the ventral tegmental area in Parkinson's disease. Front. Aging Neurosci. 15 https://doi.org/10.3389/fnagi.2023.1187684.

Zhao, X., An, H., Liu, T., et al., 2017. Quantitative susceptibility mapping of the substantia nigra in Parkinson's disease. Appl. Magn. Reson. 48 (6), 533–544.

Zhou, L., Li, G., Zhang, Y., et al., 2021. Increased free water in the substantia nigra in idiopathic REM sleep behaviour disorder. Brain 144 (5), 1488–1497. https://doi.org/10.1093/brain/awab039.